UNITED STATES
DEPARTMENT OF THE INTERIOR
GEOLOGICAL SURVEY

INTERAGENCY REPORT #64

LAVA FLOWS IN MARE IMBRIUM: AN EVALUATION OF ANOMALOUSLY LOW EARTH-BASED RADAR REFLECTIVITY

Gerald G. Schaber*, Thomas W. Thompson**,

and Stanley H. Zisk***

December 1974

This report is preliminary and has not been edited or reviewed for conformity with U.S. Geological Survey standards and nomenclature.

Prepared by the Geological Survey for the National Aeronautics and Space Administration

INTERAGENCY REPORT #64

LAVA FLOWS IN MARE IMBRIUM: AN EVALUATION OF ANOMALOUSLY LOW EARTH-BASED RADAR REFLECTIVITY

Gerald G. Schaber*, Thomas W. Thompson**,

and Stanley H. Zisk***

December 1974

(Submitted for publication in the Journal The Moon)

---

* U.S. Geological Survey, Branch of Astrogeologic Studies; Flagstaff, Arizona 86001. Work performed under NASA sponsored Apollo experiments S-217 and S-222. Funding by S-222.

** Jet Propulsion Laboratory, 4800 Oak Grove Drive; Pasadena, California 91103. Work performed under Apollo experiment S-217 and contract NAS7-100.

*** Massachusetts Institute of Technology, Haystack Observatory; Westford, Massachusetts 01886. Work performed under Apollo experiment S-217.

ABSTRACT

The lunar maria reflect 2 to 5 times less Earth-based radar power than the highlands with the spectrally blue maria surfaces returning the very lowest power levels. This effect of weakening signal return has been attributed to increased signal absorption related to the electrical and magnetic characteristics of the mineral ilmenite ($FeTiO_3$).

The surface of Mare Imbrium contains some of the most distinct red-blue colorimetric boundaries and depolarized 70 cm wavelength reflectivity variations on the near side of the Moon. The weakest levels of both 3.8 cm and 70 cm reflectivity within Imbrium are confined to regional mare surfaces of the blue spectral type that can be recognized as stratigraphically unique flow surfaces. Frequency distributions of the 70 cm polarized and depolarized radar return power for five mare surfaces within the basin indicate that signal absorption, and probably the ilmenite content, increases generally from the earliest Imbrian period to the latest Eratosthenian period. A slight reversal between the latest Imbrian and earliest Eratosthenian periods can also be noted.

TiO_2 calibrated radar reflectivity curves can be utilized for lunar maria geochemical mapping in the same manner as the TiO_2 calibrated spectral reflectivity curves presented by Charette et al. (1973). The long wavelength radar data may be a sensitive indicator of mare chemical variations since it is unaffected by the normal surface rock clutter that includes ray materials from large impact craters.

1: INTRODUCTION

The surface of Mare Imbrium contains some of the most distinct "red-blue" colorimetric boundaries and depolarized 70 cm radar backscatter variations on the near side of the Moon. Even though they are obtained at greatly diverse electromagnetic frequencies, a surprisingly good correlation exists between these two data sets. In the present investigation we integrate detailed stratigraphic information for the Imbrium basin with available radar and color data in order to establish the physical and/or chemical relationships between distinct mare surfaces, radar reflectivity and spectral color data.

A number of the color boundaries within Imbrium were shown by Strom (Kuiper, 1965; Whitaker, 1972) to correlate with the scarps of relatively young lava flows recently mapped in detail by Schaber (1973). The association of these lava flows with weak depolarized radar return at 70 cm was reported earlier by Schaber et al. (1972).

The radar data were produced by transmitting circularly polarized radiation and by analyzing the returned signal into (1) a component polarized opposite to that of the original pulse, and (2) a component with polarization the same as that of the original pulse. The first is called the "polarized" signal, since it has the polarization expected from a specular reflector (perfectly smooth sphere), and the second component is called the "depolarized" signal which is orthogonal to the polarized component. A detailed account of the Doppler-delay radar mapping technique can be found in Pettingill et al. (1974); Thompson and Zisk, (1972); and Zisk et al. (1974).

Two distinct physical processes are responsible for the observed echoes (Rea et al., 1964; Hagfors, 1967; Pettengill et al. , 1974). The first process is called quasi-specular reflection, in which the echoes are highly polarized and show a sharp decrease of power with increasing angle of incidence. The major portion of the radar echo is of this type, and it has been attributed to scattering from a large number of smooth facets many wavelengths in size, oriented normal to the radar signal (Brown, 1960). The second process, diffuse scattering, accounts for all of the polarized echoes and most polarized echoes beyond angles of incidence of 40 degrees. Diffuse scattering is generally thought to be caused by single or multiple scattering of radar echoes by rocks on the surface and/or within the upper few meters of the regolith (Hagfors, 1967; Burns, 1970; Thompson and Zisk, 1972; Pollack and Whitehill, 1972).

Thompson et al. (1974) have shown that greatly enhanced depolarized 3.8 cm and 70 cm radar signals can be correlated with the increased roughness of fresh impact craters (crater walls and blocky ejecta). We suggest here that weaker-than-normal mare backscatter is caused by an entirely different process involving increased signal absorption within the regolith; this being related to the effect of ilmenite ($FeTiO_3$)on increasing electrical and magnetic losses in the material.

We agree with Pollack and Whitehill (1972) that the observed 1:2 difference in returned depolarized power from the lunar mare and highlands, respectively, is a measure of the absorption properties of the surface materials and are probably caused by increasing concentrations of ilmenite from gabbroic-anorthosite (highlands) to titaniferous basalt (maria) materials. Evidence is presented to show that the real, but little

understood, effect of Ti-Fe chemistry on the radar absorption is so sensitive that distinct, intramare surfaces mapped within Mare Imbrium can be clearly delineated by analysis on the frequency distribution of returned radar power.

2: RADAR REFLECTIVITY IN MARE IMBRIUM

The areas of weakest* 70 cm polarized and depolarized backscatter in Mare Imbrium all fall on spectrally blue mare surfaces of both Imbrian and Eratosthenian age (Fig. 1a, b, c) (Wilhelms and McCauley, 1970; Schaber, 1969, 1973). Although the weak return areas on the polarized map are discontinuous and less pronounced than on the depolarized map, the correlation between low radar return and blue mare is obvious on both maps. We can assume that the weakest returns on the polarized map can be chiefly attributed to a local decrease in the parameters responsible for diffuse scattering since the reduction in signal is even more pronounced on the depolarized map (Pettengill and Thompson, 1968; Thompson and Zisk, 1972; Thompson, 1974).

*The backscatter levels indicated in figure 1b,c, are >50 percent down in power from the average blue mare characteristic of the west side of the basin and >75 percent down in power from the average red mare of Imbrian age that occupies much of the eastern half of the basin. The above levels of backscatter will hereafter be referred to as weak return for convenience.

Figure 2 is a black and white print of a UV-IR color composite photograph** of the Mare Imbrium region for comparison with figures 1a, b. A

correlation does exist between the below-average levels of 70 cm depolarized backscatter and the blue mare surfaces of both Imbrian and Eratosthenian age within the basin. However, on the UV-IR composite photograph, none of the individually mapped blue mare surfaces shown on figure 1a can be delineated where they are in contact with one another. The rather poor separation of the blue mare surfaces on the UV-IR map (fig. 2) is also seen in figures 3a, b which show the relative blue-red spectral reflectivity of two Imbrian and three Eratosthenian surfaces scanned from a digitized version of the figure 2 photograph. The areas scanned are shown in figure 4. Note that blue mare surfaces of both the Imbrian and Eratosthenian age have about the same relative blueness whereas the Imbrian red surface is shifted considerably to the red. The slight increase in redness shown by the Eratosthenian Phase-III is thought to be an effect of abundant aluminum-rich, Copernicus ray materials in southern Mare Imbrium. The distribution of weak return levels of depolarized radar power thus appears to be a better discriminator of these mappable flow surfaces than the currently available colorimetric photography. A new set of higher resolution red-blue color maps will soon be available and these might prove to be better discriminators of the individual blue flows (Whitaker, 1974).

**Courtesy of Ewen Whitaker (Lunar and Planetary Laboratory, University of Arizona, Tucson, Arizona).

The agreement of 70 cm polarized and depolarized weak return with geologically mapped flow units is best seen in the region of the youngest Eratosthenian age eruptives shown in figures 5a, b, c and indexed in figure 1a. It is clear that a large concentration of depolarized weak return data

lies within the boundaries of the Phase-III lavas as the youngest eruptives in the basin. The depolarized weak return data labeled "A" (fig. 5c) closely follows the most extensive (400 km) flow of that eruptive sequence. A significant number of the smaller, isolated, weak return areas correlate with blue Phase-II surfaces while still others are associated with blue materials of Imbrian age. Note how both the polarized and depolarized weak return data are absent from the red mare patches (labeled "R").

Figure 6 (same map base as figures 5a, b, c) shows the distribution of depolarized weak return data at the 3.8 cm wavelength. Although the 3.8 cm weak return data are spotty due to the nature of surface backscatter at this shorter wavelength, they do follow closely those observed at 70 cm, tending to concentrate on the very youngest (Phase-III) blue lavas of Eratosthenian age and clearly are absent from the underlying red mare surfaces. The shorter wavelength maps show much more variability since the short wavelengths are more sensitive to background "noise" caused by higher population of 1 to 10 cm size surface rocks and small, fresh, primary and secondary craters. Also, these small craters are more visible in the finer resolution 3.8 cm wavelength maps. Ray materials from the young craters Copernicus, Aristarchus and Aristillus are very distinct in the 3.8 cm maps but are not seen in the 70 cm data.

There is an excellent correlation of the 3.8 cm depolarized weak return data with the small flow labeled "X" on figure 6. This particular flow is not well defined on the depolarized 70 cm data (fig. 5c).

3: RADAR POWER FREQUENCY DISTRIBUTIONS

Digital radar images of five distinct Imbrian and Eratosthenian age surfaces within Mare Imbrium (fig. 4) were processed to show areal distributions of polarized and depolarized 70 cm radar power (figs. 7a, b,

c). The three Eratosthenian surfaces are of the blue spectral type whereas the oldest Imbrian age surface is extremely red, the youngest quite blue.

Table 1 shows that the average power decreases with the youth of the surface both in the Imbrian and Eratosthenian periods. The young Eratosthenian Phase-III lava flows, shown earlier to possess the best correlation with lowest levels of 3.8 cm and 70 cm backscatter, are seen on the table to reflect only 56 percent of the average mare on the depolarized maps and 70 percent of the average polarized mare return. The Imbrian red mare, on the other hand, reflects one percent more than average polarized return for the basin and nineteen percent more than the average depolarized value for the basin.

The average power return for these surfaces is, however, rather misleading since it is in the low end of the return power scale that the various surfaces appear to be best differentiated. Figure 8 compares the percent of radar return power below the 50 percent level with cumulative percent of surface area for one Imbrian (Imbrian blue) and three Eratosthenian (Phase I, II, and III) blue geologic units. The Imbrian red region (fig. 4) has no return below the 58.5 percent level and therefore is not included.

The Eratosthenian Phase III eruptives are clearly the poorest radar reflectors with 40.7 percent of the surface returning less than 50 percent of the average depolarized radar power for the basin. Phase III is followed by Phase II with 23.3 percent, Imbrian blue with 13.9 percent and Phase I with 9.3 percent (Table 1).

4: SURFACE AND SUBSURFACE ROCKS

Differences in the depolarized radar signals have been attributed to variations in the distribution of wavelength size structures, notably rocks, and/or in the ability of the surface layer to absorb the incident radiation and thereby affect the strength of echoes returned from the subsurface (Thompson et al., 1973; Pieters, et al., 1973; Pollack and Whitehill, 1972).

Thompson et al. (1974) made the assumption that the 3.8 cm radar detects rocks which range in size from 1 cm to 40 cm and are on the surface or buried no deeper than 1 m. Similarly, the 70 cm radar detects those rocks which range in size from 20 cm to 7 m and are on the surface or buried no deeper than about 20 m. Surveyor television images and Apollo lunar surface photography have confirmed that rocks ranging in size from 25 cm and up are rare. Rocks in the size range effective to the 70 cm radar are generally associated only with ejecta from relatively large (>300 m diameter) impact craters that penetrate the regolith. The average cumulative frequency of rocks in the size range 1 cm to 10 m published for various Surveyor and Apollo mare sites reveal that the rock populations on diverse mare surfaces vary little and that an average mare surface contains about 200 times as many 1 cm rocks than 10 cm rocks and 5 times as great a number of 25 cm size boulders than 50 cm boulders (Shoemaker et al., 1968; Shoemaker et al., 1970a; Shoemaker et al., 1970b; Muehlberger et al., 1972). The mechanism causing the relatively high average 3.8 cm diffuse backscatter across the Imbrium basin may therefore be partially due to this normally large population of 1-20 centimetre-sized rock fragments unseen by the 70 cm signals.

We have shown that the blue mare surfaces within Mare Imbrium have a highly reduced depolarized radar return, especially at the 70 cm wavelength. If rock populations are the sole cause of depolarized radar variations, the inference is that abnormally low rock populations (>20 cm) characterize these surfaces. We will show that this is probably not the case.

Thompson et al. (1974) have suggested that increased lunar eclipse infrared temperatures associated with fresh impact craters are controlled by the abundance of surface rocks greater than 10 cm diameter; they further showed that photogeologic evidence and increased 3.8 cm and 70 cm radar backscatter data confirm this hypothesis. However, the interpretation of the regional variation in mare eclipse temperatures are the subject of considerable debate (Hunt et al., 1968; Buhl, 1971; Hagfors, 1970; Winter, 1970).

A modified 11 micron eclipse temperature image of the Imbrium basin shown in figure 9 suggests that the Eratosthenian lava flows have slightly higher surface temperatures (5-10 degrees K) than the older Imbrian materials. These data show the departures in temperature from an average temperature for the region (Shorthill, 1973).

If increased rock populations are the cause of the regional mare eclipse temperature increases as previously suggested, then, what is the cause of the reduced radar backscatter? The major differences between the eastern and western lunar maria are the lower average albedo (Pohn et al., 1970) and suspected higher titanium and iron content in the western hemisphere maria (Boyce et al., 1974). One need only compare the eclipse IR data (fig. 10a) and the full Moon lunar albedo (fig. 10b) to observe a generally good correlation of low albedo and increased temperature

within the lunar maria (Moore, 1974). It appears, then, that these two data sets are not reflecting the abundance of 10 cm and larger surface rocks but instead, the distribution of surfaces with unusually low thermal inertias associated with lower visible albedo. On a local scale, of course, elevated thermal and albedo values can be related to the blocky ejecta and walls of large impact craters. Variations in lunar surface color have been shown to be intimately associated with changes in lunar albedo (low albedo blue color; high albedo red color), both being related to chemical differences involving, primarily, titanium and iron.

5: SURFACE SLOPE VARIATIONS

Differences in root mean square (rms) surface slopes on the various mare units within Imbrium are not suspected as being a major factor in the observed radar behavior since the depolarized data from the blue surfaces reveals a sharp decrease in return power over the polarized return. The depolarized data, as stated earlier, contains primarily the diffuse component of the radar echo and little or no quasi-specular echo component, expected from gentle surface undulations.

There are however distinct kilometre-scale surface textural differences that can be observed on low Sun Apollo photography between the Imbrian blue and Eratosthenian Phase-III surface (fig. 11). Utilizing the photoclinometric technique (Rowan and McCauley 1966) we found the former to have an average rms slope of 0.6 degrees, the latter 0.4 degrees, at a 3 km slope length scale.

Variations in surface slope at this scale are thought to be associated with smoothing of an underlying cratered surface by a younger eruptive

sequence. Schaber et al. (1970) discussed the distinct association of flooded craters (1-4 km diameter size) with weak radar return from the blue Eratosthenian surfaces in northern (Phase-I) and central (Phase-II) Imbrium. Further investigation of such flooded craters revealed that their numbers decrease with youth of the eruptive sequence, suggesting complete burial of all Imbrian age craters and early Eratosthenian age craters less than 4 km (diameter) (150 m rim height) by the time of the lastest Phase-III deposition.

We have, at present, no way of determining if the kilometre-scale surface slope variations within Imbrium can be extrapolated down to the radar wavelength scales of 3.8 cm and 70 cm; but Surveyor and Apollo surface photography suggests little consistent textural difference below the metre scale for all visited mare sites which represents a 0.5 b.y. year range in age (including the Apollo 17 site).

6: CRATER SIZE FREQUENCY DISTRIBUTIONS WITHIN IMBRIUM

The crater size frequency distribution of five mare surfaces within Imbrium are shown in figures 12a,b. Due to the absence of high-resolution photography north of 32°N, only the Phase-III crater counts were extended down to the 25 m diameter crater size. When the statistical error bars are considered, all of the blue surfaces (Imbrian blue and Phases I, II and III) are extremely close in >250 m diameter crater populations. The old Imbrian red surface, characteristic of the eastern half of the basin, appears to be about 2 times more cratered than the average blue mare in the >250 m diameter crater size range.

The frequency distribution of craters <150 m diameter for the young Phase-III flows is especially interesting since the number of craters

decreases more rapidly than predicted by the steady state crater curve (Shoemaker et al., 1968). These data are in agreement with recent findings of Howard et al. (1973) in Mare Serenitatis where the low albedo, blue, outer ring mare of that basin has been found to be older than the central red mare, contrary to pre-Apollo 17 concepts (Wilhelms and McCauley, 1971). Although older, the blue ring mare has fewer <150 m diameter craters than the red central mare and its crater size frequency curve crosses that of the latter at about the 150 m diameter crater size (Wolfe, 1974).

There is then some evidence that the blue maria, on a lunarwide scale, may have fewer craters <150 m diameter than red maria, regardless of their age relationships. There appears then to be a poorly understood physical process, innate to the blue mare and dark mantled areas, that preferentially destroys small craters on these surfaces much more rapidly than on the red mare surfaces. This parameter is being investigated at the Apollo 17 site where it may be caused by an anomalously thick unconsolidated layer (30 m; Wolfe, 1974) generated perhaps as a pyroclastic deposit and/or as a frothy upper flow surface resulting from rapid degassing of a basalt liquid, particularly high in titanium and volatiles.

7: REGOLITH CHARACTERISTICS

There is some weak evidence suggesting that the regolith on the blue mare surfaces within Imbrium is anomalously thick as much as 2.5 times that expected by impact comminution of a coherent substrate. Figure 13 relates increased depths of regolith with relative crater erosion ages for several Surveyor and Apollo landing sites utilizing the mare dating method of

Soderblom and Lebofsky (1970)* and additional data from Boyce et al. (1974); Swann et al., (1972, 1974); Shoemaker et al. (1970a) and Moore (1974). Listed also on figure 13 are the D_L values given by Schaber (1973) and Boyce (1974) for various mare surfaces mapped within Imbrium. Note that for the latter, the predicted regolith depths vary from 5.2 m to 3.0 m, from the oldest to the youngest.

*The method involves visual examination of an orbital photograph to determine the maximum diameter of craters (D_s) whose internal slopes have been reduced to slopes less than the Sun elevation (S_s). Utilizing the Soderblom (1970) model of small crater impact erosion, measurements of D_L are converted to an equivalent diameter (D_L) of a crater eroded to an interior slope of one degree under the same flux which has eroded a crater of diameter D_s to a slope of S_s. Values of D_L are considered synonymous with relative age which is directly proportional to the total number of craters that have accumulated on the surface.

Quaide and Oberbeck (1968), using a statistical method based on small crater morphology, calculated an average 7.5 m regolith depth for a region 32° N22°W) including both an Imbrian blue and Eratosthenian Phase-III surface. This value is 1.9 to 2.5 times larger than the expected normal depths for these flow surfaces shown on figure 13. The regolith thicknesses for these same two surfaces plus a Phase-II surface were rechecked utilizing the Quaide and Oberbeck method. Values of 5 m, 10 m, and 8 m were found for the Imbrian blue, Phase-II and Phase-III surfaces, respectively, agreeing well with the earlier Quaide and Oberbeck data (Walker, 1974). The important point is that

at least the youngest blue lava surfaces within the Imbrium basin (Phase-II and Phase-III) may have slightly greater apparent regolith depths and weak radar return as well.

Fielder and Fielder (1971) supplied additional evidence for the presence of a more compressible, and possibly thicker, regolith on the northernmost terminus (32° N,22° W) of the young Phase-III lava flows*. They pointed out the existence of a unique type of double-rimmed or benched craters on the Phase-III flow using Lunar Orbiter V high resolution photography (frames H-159 and H-160). The benched craters on the Phase-III surface have a conspicious deep pit in their floor whereas those on the underlying Imbrian blue surface are characterized by a flat, rubbly floor. There are virtually none of the deep pit type on the older surface and vice versa. The presence on the young flow of the benched craters with the deep pit was attributed by Fielder and Fielder as evidence of a more compressible, frothy upper surface on the younger surface related to an abnormally rapid outgassing. The present authors agree with this hypothesis.

*Fielder and Fielder (1971) used the notations f1 and f3 for the Imbrian blue and Phase-III flows, respectively.

It is difficult to accept the possibility that slight variations in regolith depth, rock populations or small crater frequencies on the blue Imbrium flows may be solely responsible for the rather large variations in radar attenuation demonstrated from these surfaces. This is especially true since the radar attenuation is definitely unrelated to surface age when looked at on a lunarwide scale. Even within Imbrium, the older Imbrian blue surface has a greater attenuation in depolarized power than the younger Eratosthenian Phase-I surface (Table 1).

The correlation of anomalous regolith thickness, weak radar reflectivity, and blue color appear to be the result of a "fundamental" difference between the blue and red maria, their initial basalt chemistry. The chemistry, including the volatiles, affects the mode of deposition (Schaber, 1973) and is perhaps related to the rate of basalt extrusion as discussed by Nisbet and Pearce (1973) for terrestrial oceanic basalts.

8: MARE COLOR, BASALT CHEMISTRY AND RADAR ABSORPTION THEORY

We have shown that strongly reduced backscatter on both the 3.8 cm and 70 cm radar maps is associated with blue mare materials of Imbrian and Eratosthenian ages within the Imbrium basin.

The most important physical differences between visible and radar enhanced "scattering" are the effective penetration depth and the reflectivity which is a function of the size of surface scatterers. Both of these are, however, related to the wavelength and have been described by classical laws of optics (e.g. Rayleigh, Lambert, etc.). It is the attenuation by absorption of these visible and radar signals that is of importance to the present discussion. The physical mechanism generally given for the color absorption variations involves transfer of electronic charge involving Ti^{3+}, Ti^{4+} and Fe^{2+} ions in the glassy material of the agglutinates and the glasses of mare regolith (Adams and McCord, 1970; Conel and Nash, 1970; Charette et al., 1974).

Adams and McCord (1973) have recently considered additional reasons for the increased optical absorption by the glassy agglutinates to include (1) the presence of abundant finely disseminated metallic iron and other opaque phases (ilmenite most abundant) and (2) the abundance of microvesicles.

The physical mechanism responsible for radar absorption is less well understood than absorption in the visible spectrum. The degree of radar absorption by a material is a complex function given (Campbell and Ulrich, 1969) as the product of magnetic permeability and dielectric constant, and the sum of the loss tangents of the material. These parameters, in turn, are effected by permittivity, density of the material, temperature of the surface layers and macroscopic conductivity of intergrain boundaries within the material. These physical and electrical parameters are discussed within the lunar context in papers by Campbell and Ulrich (1969), Pollack and Whitehill (1972), and Alvarez (1974).

In the present discussion we have tried to characterize the results of radar behavior by showing a distinct correlation between increased absorption, blue color data, and mare stratigraphy. The positive correlation of these data sets strengthens the theory that some parameter (or parameters), related to basalt chemistry, is responsible for the radar behavior in the maria. On a lunarwide scale, the depolarized return from the basaltic mare areas is consistently lower than that of the gabbroic-anorthosite highlands by a factor of between 2 and 5 at the 70 cm wavelength (Thompson, 1974). Similar results have been reported for wavelengths ranging from 0.86 cm to 7.0 m (McCue and Crocker, 1972; Thompson, 1971).

Pollack and Whitehill (1972) in developing a physical model of lunar radar multiple-scattering suggested that the most important factor affecting the mare-highlands radar backscatter differences may be the radar absorption length in rocks and soil within the two regions--possibly related to ilmenite content. The absorption length of a material is defined as the distance over

which an electromagnetic wave must travel in the material before being attenuated to 1/e (36.8 percent) of its initial intensity. Pollack and Whitehill (1972) suggest that a change in the absorption length of a factor of only 3.5 would be required to produce a change of a factor of 5 in the depolarized lunar radar return observed between the maria and highland. Campbell and Ulrich (1969) reported absorption lengths of 7 m and 65 m in tholeiitic basalt and anorthosite powders (density=1.0 g cm^{-3}), respectively, at the 70 cm (450 Mhz) wavelength. They also reported absorption lengths of 0.4 m and 6.0 m in tholeiitic basalt and anorthosite solid rock at the 70 cm wavelength. The magnetic losses that may arise from the excessive ilmenite content in mare basalts (up to 25 percent in Apollo 17 basalts) may be a significant factor in further reducing the absorption lengths in mare materials.

A primary question is whether the 70 cm radar signals are reaching through the mare regolith into the fractured substrate basalts and, if so, where is the major absorption taking place? The absorption data of Campbell and Ulrich given above indicate that both the mare regolith and mare basalts could be highly attenuating to the signal. The 70 cm signals may be penetrating the highly absorbing mare regolith and encountering even greater attenuation in the highly titaniferous basaltic substrate.

Recent electrical properties measurements on returned Apollo 14, 16, and 17 samples by Sill (1974) have shown that the Apollo 17 (8-10 percent TiO_2) soils have significantly higher density (1.3 times), dielectric constant (1.3 times), and loss tangent (3.3 times) than those of Apollo 14 (2.0 percent TiO_2) and 16 (1.0 percent TiO_2) at a frequency of 10 Mhz. These values

appear to be increasing directly with the titanium content, with the loss tangent showing the largest and perhaps the most significant variation with regard to signal absorption. The effect of increased dielectric constant or increased density alone would be to enhance the radar backscatter from regolith surfaces; the opposite of the observed behavior.

Additional laboratory radar research will be needed before the radar absorption phenomena can be fully understood. Special attention should be placed on the electrical and magnetic effects of opaque minerals in glassy soils and basalts of the lunar type.

9: CALIBRATION OF TiO_2 AND RADAR RETURN

Charette et al. (1973) gave percent TiO_2 in bulk soils for thirteen lunar regions obtained by calibration of slopes of spectral reflectivity curves utilizing return lunar sample spectral data. Included in the telescopically obtained spectral data were two regions within Mare Imbrium, one in the red Imbrian mare at the northeastern edge of the basin (47°10'N; 9° 50'W), the other in the Phase-I Eratosthenian blue mare near the crater Helicon (38°45'N; 22°40'W) (fig. 1). They obtained a low value of 1.3 ±.5 percent TiO_2 for the red Imbrian age mare and a high 6-8 percent for the blue phase-I mare.

Utilizing these two data points within the basin and assuming a linear relationship between TiO_2 content and average backscatter power from our frequency distribution data (figs. 7a, b, c), we have established a preliminary calibration curve to estimate TiO_2 content in Mare Imbrium bulk soils (fig. 14). The important observation from this preliminary curve, however, is that Imbrian age surfaces within the basin appear to contain from 1 to 8 percent TiO_2 in bulk surface soils, whereas the Eratosthenian age

surfaces may vary from 7 to 10 percent. The Apollo 17 soils contain up to 10 percent TiO_2 (LSPET, 1973).

The authors are in the process of acquiring additional spectral reflectivity measurements within the Imbrium basin from which we can refine the calibration curve. Continuing research will also include calibration of the radar return from Apollo and Luna landing sites where physical, chemical and electrical data are available on the samples. The present lunar radar research should prove a powerful tool for lunar geochemical and geologic mapping and may be of significant value during preliminary analysis on available Doppler-delay radar maps of Venus.

10: CONCLUSIONS

The present investigation has utilized geologic, photometric, colorimetric and radar backscatter maps of Mare Imbrium to suggest a distinct association between individual basalt flows having blue color and greatly attenuated radar return. The main conclusions can be summarized as follows:

(1) Earth-based 3.8 cm and 70 cm polarized and depolarized radar return from Mare Imbrium decreases in average intensity from from the old red to younger blue Imbrian age surfaces and also decreases from the oldest to youngest Eratosthenian surfaces, all of the blue spectral type.

(2) This reduced radar backscatter from the red to the blue mare surfaces is attributed to increased radar absorption in the latter, resulting, at least indirectly, from increased titanium and/or iron content in the basalts and overlying regolith. The important physical/chemical parameter may be increased concentrations of disseminated ilmenite opaques in a slightly deeper than normal glassy regolith.

(3) Titanium calibration of Earth-based radar backscatter maps should provide a powerful new tool for lunar geochemical and geologic mapping as well as providing a means for preliminary geological and geochemical analysis of Earth-based Venus radar backscatter maps.

ACKNOWLEDGMENTS

Radar and infrared data displays and analyses were performed at the Image Processing Laboratory of the Jet Propulsion Laboratory (California Institute of Technology) under NASA contract NAS 7-100 and Apollo experiment S-217. Additional radar analyses were performed at the Haystack Observatory (Massachusetts Institute of Technology) under NASA funding to Apollo experiment S-217.

The authors thank Lyman Lyon of the Jet Propulsion Laboratory for radar display programming and the scientific illustration group and computer facility staff of the U.S. Geological Survey (Flagstaff, Arizona) for their fine support.

REFERENCES

Adams, J. B., and McCord, T. B.,1970, Remote Sensing of Lunar Surface Apollo 11 Samples , Proceedings of the Apollo 11 Lunar Science Conference: Geochem. et Cosmochim. Acta, Supl. 1, 3, 1937-1945.

Adams, J. B., and McCord, T. B., 1973, Vitrification Darkening in the Lunar Highlands and Identification of Descartes Material at the Apollo 16 site : Pub. no. 79, Mass. Inst. Tech. Planetary Astronomy Lab., 35 p.

Boyce, J. M., 1974, personal communication.

Boyce, J. M., Dial, A. L., and Soderblom, L. A., 1974, Ages of the Lunar Nearside Light Plains and Maria , Proceedings of the Fifth Lunar Science Conference: Geochim. et Cosmochim. Acta, Supl. 5., in press.

Brown, W. E., Jr., 1960, A Lunar and Planetary Echo Theory : J. Geophys. Res., 65 (10), 3087-3095.

Buhl, D., 1971, Lunar Rocks and Thermal Anomalies : J. Geophys. Res., 76 (14), 3384-3390.

Burns, A. A., 1969, Diffuse Component of Lunar Radar Echoes : J. Geophys. Res., 74 (27), 6553-6566.

Campbell, M. J., and Ulrich, J., 1969, Electrical Properties of Rocks and Their Significance for Lunar Radar Observations : J. Geophys. Res., 74 (25), 5867-5881.

Charette, M. P., McCord, T. B., Pieters, C., and Adams, J. B., 1974, Application of Remote Spectral Reflections Measurements to Lunar Geology Classification and Determination of Titanium Content of Lunar Soils : J. Geophys. Res., 79 (11), 1605-1613.

Conel, J. E., and Nash, D. B., 1970, Spectral Reflectance and Albedo of Apollo 11 Lunar Samples--Effects of Irradiation and Vitrification and Comparison with Telescopic Observations : Proceedings of the Apollo 11 Lunar Science Conference: Geochim. et Cosmochim. Acta., Supl. 1, 3, 2013-2023.

Fielder, G., and Fielder, J., 1971, Lava Flows and the Origin of Small Craters in Mare Imbrium , Chapter 2: Geology and Physics of the Moon (G.Fielder, ed.), Elsevier, 15-26.

Hagfors, T., 1967, A Study of the Depolarization of Lunar Radar Echoes : Radio Sci., 2 (5) (new series), 445-465.

Hagfors, T., 1970, Remote Probing of the Moon by Infrared and Microwave Emissions and by Radar : Radio Science, 5 (2), 189-227.

Howard, K. A., Carr, M. H., and Muehlberger, W. F., 1973, Basalt Stratigraphy of Southern Mare Serenitatis: Apollo 17 Preliminary Science Report; NASA SP-330, National Aeronautics and Space Administration, 29-1 to 29-12.

Hunt, G. R., Salisbury, J. W., and Vincent, R. K., 1968, Lunar Eclipse Infrared Images and an Anomaly of Possible Internal Origin : Science, 162, 252-254.

Kuiper, G. P., 1965, Interpretation of Ranger VII Records , Ranger VII, pt. II, Experimenters' Analyses and Interpretations: Jet Propulsion Lab. Tech. Rept. 32-700, 9-73.

Lunar Sample Preliminary Examination Team, 1973, Preliminary Examination of Lunar Samples: Apollo 17 Preliminary science Report; NASA SP-330, National Aeronautics and Space Administration, p. 7-1 to 7-46.

Moore, H. J., 1974, personal communication of work in progress.

Nisbet, E., and Pearce, J. A., 1973, TiO_2 and a Possible Guide to Past Oceanic Spreading Rates : Nature, 246, 468-470.

Oberbeck, V. R., and Quaide, W. L., 1968, Genetic Implications of Lunar Regolith Thickness Variations : Icarus (9), 446-465.

Pettengill, G. H., Zisk, S. H., and Thompson, T. W., 1974, The Mapping of Lunar Radar Scattering Characteristics : The Moon, 10, 3-16.

Pettengill, G. H., and Thompson, T. W., 1968, A Radar Study of the Lunar Crater Tycho at 3.8 cm and 70 cm wavelengths : Icarus, 8 (3), 457-471.

Pieters, C., McCord, T. B., Adams, J. B., and Zisk, S. H., 1973, Lunar Black Spots and Nature of the Apollo 17 Landing Site : J. Geophys. Res., 78 (26), 5867-5875.

Pohn, H.A., Wildey, R.L. and Sutton, G.E., 1970, A Photometric-Photographic Study of the Normal Albedo of the Moon : Geol. Surv. Prof. Paper 599-E: U.S. Printing Office, Washington, D. C., 20 p.

Pollack, J. B., and Whitehill, L., 1972, A Multiple-Scattering Model OF THE Diffuse Component of Lunar Radar Echoes : J. Geophys. Res., 77 (23), 4289-4303.

Rea, D. G., Hetherington, N., and Mifflin, R., 1964, The Analysis of Radar Echoes from the Moon : U.S. Geol. Survey Misc. Map Series, I-602.

Schaber, G. G., 1969, Geologic Map of the Sinus Iridum Quadrangle of the Moon : U.S. Geol. Survey Misc. Map Series, I-602.

Schaber, G. G., 1973, Eratosthenian Volcanism in Mare Imbrium--Source of Youngest Flows : Apollo 17 Preliminary Science Report; NASA SP-330, National Aeronautics and Space Administration, 30-17 to 30-25.

Schaber, G. G., 1973, Lava Flows in Mare Imbrium: Geologic Evaluation From Apollo Orbital Photography: Proceedings of the Fourth Lunar Sci. Conf.: Geochem. et Cosmochim. Acta, Supl. 4, 73-94.

Schaber, G. G., Thompson, T. W., and Eggleton, R. E., 1972, Lunar Radar Mapping Correlation between Radar Reflectivity and Stratigraphy in Northwestern Mare Imbrium : Nature, 226, 1236-1239.

Shoemaker, E. M., et al., 1970a, Lunar Regolith at Tranquillity Base : Science, 167, 3918, 452-455.

Shoemaker, E. M., et al., 1968, Television Observations from Surveyor: in Surveyor Project Final Report, pt. II--Science Results: Jet Propulsion Lab. Tech. Rept. 32-1265, 21-136.

Shoemaker, E. M., et al., 1970b, Preliminary Geologic Investigation of the Apollo 12 Landing Site, Pt. A--Geology of the Apollo 12 Landing Sites: Apollo 12 Preliminary Science Rept.: NASA SP-235, National Aeronautics and Space Administration, 113-156.

Shorthill, Richard W., 1973, Infrared Atlas Charts of the Eclipsed Moon : The Moon, 7 (1/2), 22-45.

Sill, W. R., 1974, personal communication, work in progress.

Soderblom, L. A., and Lebofsky, L. A., 1972, Technique for Rapid Determination of Relative Ages of Lunar Areas from Orbital Photography: J. Geophys. Res., 77, 279-296.

Soderblom, L. A., 1970, A Model for Small Impact Erosion Applied to the Lunar Surface : J. Geophys. Res., 75 (14), 2655-2661.

Swann, G. A., et al., 1972, Preliminary Geologic Investigation of the Apollo 15 Landing Site : Apollo 15 Preliminary Science Report NASA SP-289, National Aeronautics and Space Administration, 5-1 to 5-112.

Swann, G. A., et al., 1974, Geology of the Apollo 14 Landing Site in the Fra Mauro Highlands : U.S. Geol. Survey Prof. Paper (in press).

Thompson, T. W., and Zisk, S. H., 1972, Chapter 1c in Thermal Characteristics of the Moon : v. 28, Progress in Aeronautics and Astronautics, M.I.T. Press, Cambridge, Mass., 83-117.

Thompson, T. W., 1974, Atlas of Lunar radar Maps at 70 cm Wavelength : The Moon, 10, 51-85.

Thompson, T. W., et al., 1973, Remote Sensing of Mare Serenitatis : Apollo 17 Preliminary Science Report ; NASA SP-330, National Aeronautics and

Walker, A., 1974, personal communication.

Whitaker, E. A., 1972, Lunar Color Boundaries and their Relationship to Topographic Features--a preliminary survey : The Moon, 4, 348-355.

Whitaker, E. A., 1974, personal communication of work in progress.

Wilhelms, D. E., and McCauley, J. F., 1971, Geologic Map of the Near Side of the Moon : Geologic Atlas of the Moon, Near Side of the Moon I-703: U.S. Geol. survey., Washington, D. C.

Winter, F., 1970, The Infrared Moon--interpretations and implications : Radio Science, 5 (2), 229-240.

Wolfe, E. W., 1974, personal communication of work in progress.

Zisk, S. H., Pettengill, G. H., and Catuna, G. W., 1974, High-Resolution Radar Maps of the Lunar Surface at 3.8 cm wavelength : The Moon, 10 (1), 17-50.

ILLUSTRATIONS

Figure 1a. A portion of Mare Imbrium showing distribution of Eratosthenian and Imbrian age mare surfaces (Wilhelms and McCauley, 1971; Schaber, 1973). Eratosthenian age surfaces are shown within solid outlines and are designated as phase I, II, or III, (III youngest). Lines with hatchures indicate maximum extent of phase-II and III lava flow scarps described by Schaber (1973). All Eratosthenian age mare surfaces are of the blue spectral type. Colorimetric properties of Imbrian age surfaces shown by B (blue), MB (medium blue), MR (medium red) and R (red). Color data taken from composite UV-IR photograph (see figure 2). Arrows indicate direction of lava flow movement. The center of the Imbrium basin is indicated. Dashed area is discussed in text (figures 5a, b, c).

Figure 1b. Portion of Mare Imbrium showing the distribution of polarized 70 cm radar return with less than 50 percent the average power for the basin (black areas). (Figure 1a caption for colorimetric information, description of mapped areas, and other symbols.)

Figure 1c. Portion of Mare Imbrium showing distribution (stippled areas) of depolarized 70 cm radar return with less than 50 percent the average power for the basin. Note excellent agreement of weak radar return from phase III flows (fig. 1a). Description of mapped areas and other symbols same as figure 1a.

Figure 2. Black and white version of a composite infrared and ultraviolet photograph showing distribution of red (light tones) and blue(dark tones) mare surfaces within Mare Imbrium. Photograph courtesy of Ewen Whitaker (Lunar and Planetary Laboratory, University of Arizona). Compare with figure 1c.

Figure 3a. Surface area distribution of relative blue-red spectral reflectivity for the Eratosthenian age (Phase I, II, and III) surfaces within Mare Imbrium. Areas scanned (figure 4) from a digitized version of the UV-IR color map shown in figure 2. The blues (0) and reddest (100) values represent the highest and lowest film density values measured within each area.

Figure 3b. Surface area distribution of relative blue-red spectral reflectivity for the Imbrian age red and blue mare surfaces within Mare Imbrium. Areas scanned shown in figure 4. See caption of figure 3a for additional information.

Figure 4. Areas within Mare Imbrium used to generate the data presented in figures 3a and b, and figures 7a, b, and c. Small stipple--Imbrian red surface; large stipple--Imbrian blue surface; left slant symbol--phase-I; right slant symbol--phase-II; cross hachured--phase-III (figures 1a, b, and c and figure 2).

Figure 5a. Photogeologic map of late Eratosthenian age lava flows in southwestern Mare Imbrium (after Schaber, 1973). Hachured lines mapped on flow scarps (barbs point downslope). Arrows indicate position of flow channels and flow direction. Solid lines with double triangles on mare ridge crest. Dashed lines with bar and ball indicate fault (ball on downthrown side). Areas labeled "R" are red mare (discussed in text); all mapped surfaces are blue. Photobase mosaic composed of rectified Apollo 15 oblique metric photographs (1553, 1556, and 1557). (Rectification by the U.S. Army Map and Topographic Command under NASA contract.)

Figure 5b. Sketch map of figure 5a photogeologic map showing correlation of weak, polarized 70 cm radar return (vertical bars) and Eratosthenian age lava eruptives. Phase II flows (cross bars); Phase-III flows (stippled). See figure 5a explanation for other symbols. Radar return shown represents levels less than 50 percent of the Imbrium basin average.

Figure 5c. Sketch map of figure 5a photogeologic map showing correlation of weak, depolarized 70 cm radar return (vertical bars) and late Eratosthenian age lava eruptives. Flow age symbols save as given in figure 5b. Radar return shown represents levels less than 50 percent of the Imbrium basin average. Symbol "A" discussed in text. The resolution cell (10 km X 10 km) of the 70 cm radar is shown.

Figure 6. Sketch map of the figure 5a photogeologic map showing correlation of weak, depolarized 3.8 cm radar return (black areas) and late Eratosthenian age lava flows. Flow age and other symbols same as given in figure 5a, b. Symbols "X" and "Y" discussed in text.

Figure 7a. Surface area distribution of 70 cm polarized return power for surfaces I, II, and III. Surfaces represented are shown in figure 4. Power levels are given relative to Imbrium basin average of 100. Vertical line (with number) through each peak indicates the average level of power returned from each surface.

Figure 7b. Surface area distribution of 70 cm depolarized return power for surfaces I, II, and III. See figure 7a caption.

Figure 7c. Surface area distribution of 70 cm polarized and depolarized return power for surfaces Imbrian blue and Imbrian red. See caption for figure 7a.

Figure 8. Cumulative area percent of blue mare surfaces within Mare Imbrium characterized by less than 50 percent of the average depolarized return for the basin. Surfaces represented shown in figure 4.

Figure 9. Distribution of Mare Imbrium surface temperatures 5 degrees K warmer than average for the basin; obtained from eclipse thermal (11 microns) Eratosthenian mare surfaces described in figure 1a. Thermal anomalies related to impact craters or ray material have been removed.

Figure 10a. Infrared map of the moon showing normalized eclipse temperatures Observers R. W. Shorthill and J. M. Saari. Lunar segments shown are LAC chart quadrangles shown on orthographic project.

Figure 10b. Distribution of lowest levels (.074 to .090) of absolute visible albedo on the Lunar Earthside hemisphere (modified from Pohn et al., 1970). Compare with elevated mare temperatures shown in figures 9 and 10a.

Figure 11. Enlargement of Apollo 15 metric photograph (1557) showing Phase-III(A) and Imbrian blue (B) areas photometrically scanned for photoclinometric calculations of rms surface slopes. Number and lines represent Sun elevation angles in degrees. Area shown about 90 km west of Mt. La Hire (fig. 5a).

Figure 12a. Crater size frequency distribution for the Eratosthenian Phase-I, II, and III surfaces within Mare Imbrium. Phase III crater counts are extended down to 25 m diameter owing to availability of high-resolution photography. The steady-state crater curve and the production crater curves of Apollo 11, 12, and Surveyor VII (Tycho Crater rim) are also shown. Statistical error bars are included.

Figure 12b. Crater size frequency distribution for the Imbrian red and Imbrian blue surfaces within Mare Imbrium. See explanation for figure 12a.

Figure 13. Apparent regolith depths related to the surface crater erosion model age (D_L) of various Surveyor and Apollo sites; as described by Soderblom and Lebofsky (1970) and Boyce et al. (1974). See text for definition of D_L and a discussion of their method of mare surface age dating. The Mare Imbrium flow surfaces discussed here are indicated on the curve.

Figure 14. Preliminary attempt at relating TiO_2 content in bulk regolith soils to mean 70 cm depolarized return power for the five Imbrian and Eratosthenian study areas within Mare Imbrium. Mean return power for Basin given as 100. Calibration of TiO_2 values limited to Phase I and Imbrian red surfaces after data given by Charette et al. (1973).

TABLES

Table 1. 70-cm polarized and depolarized radar statistics for two Imbrian and three Eratosthenian age mare surfaces within Mare Imbrium. All data in columns 1 and 3 are relative to the average radar return for the basin of 100.

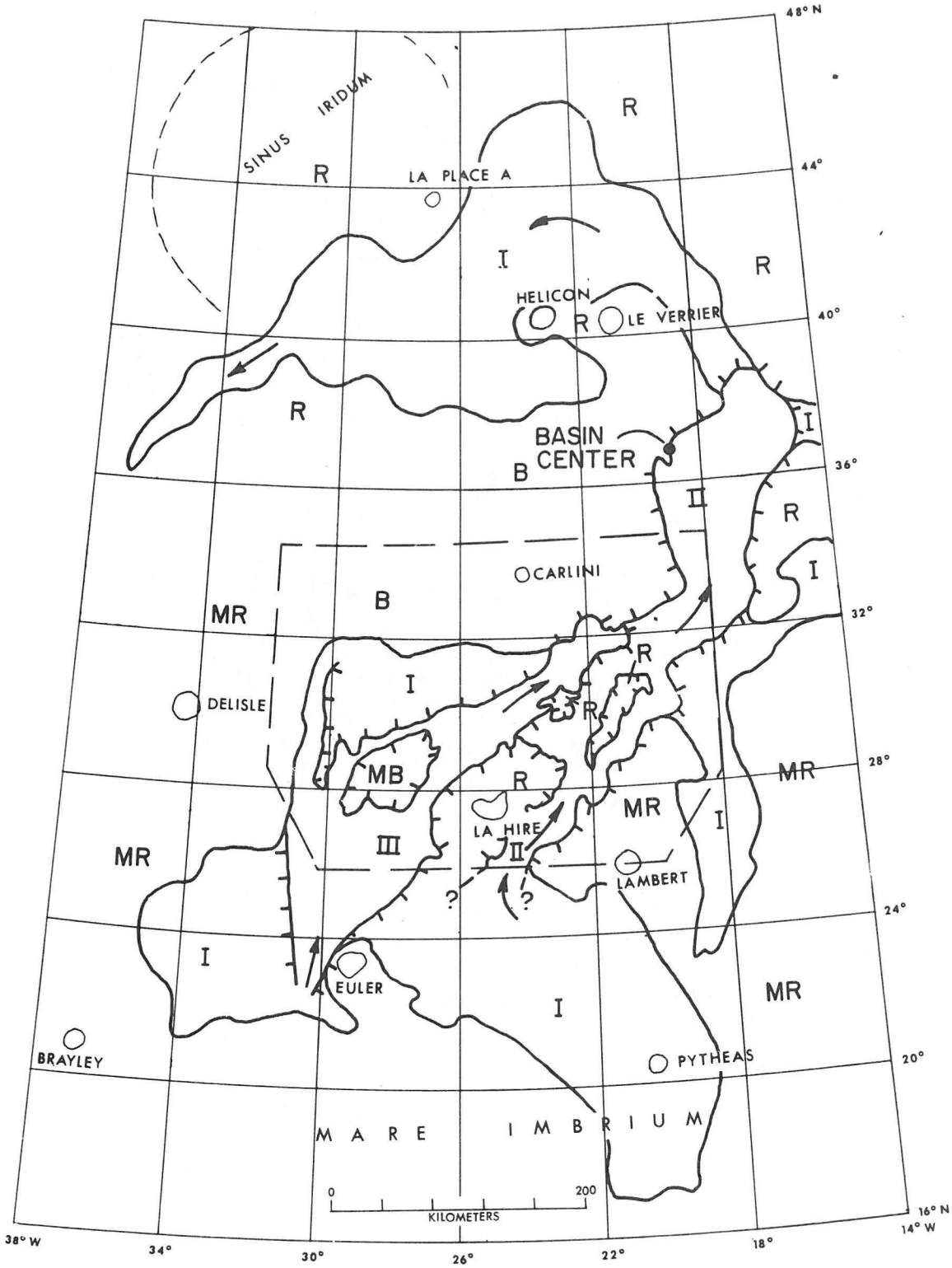
SINUS IRIDUM
LA PLACE A
HELICON
LE VERRIER
BASIN CENTER
CARLINI
DELISLE
LA HIRE
LAMBERT
EULER
BRAYLEY
PYTHEAS
MARE IMBRIUM
KILOMETERS
0
200
48° N
44°
40°
36°
32°
28°
24°
20°
16° N
14° W
38° W
34°
30°
26°
22°
18°

Figure 1a.

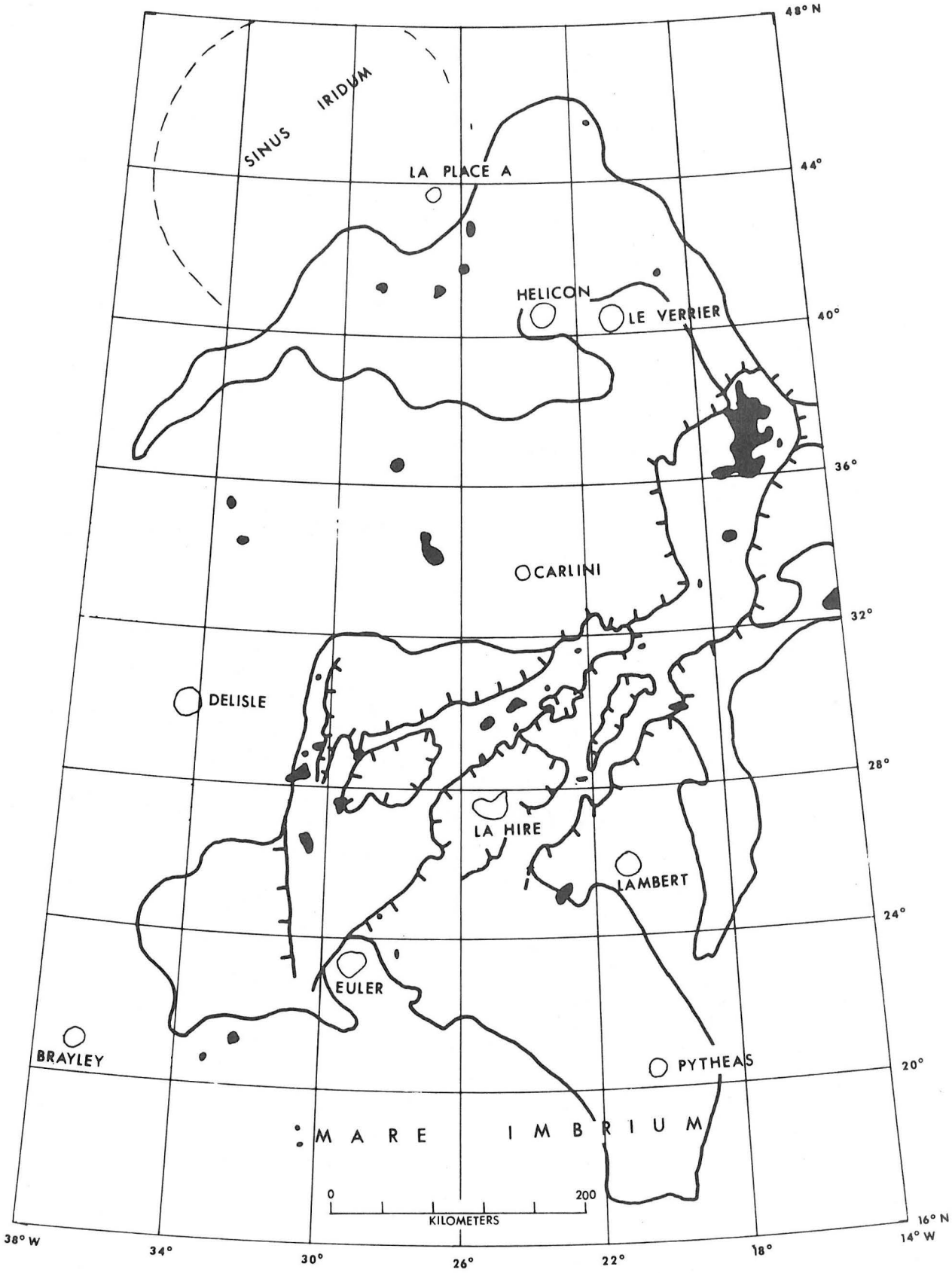
SINUS IRIDUM
LA PLACE A
HELICON
LE VERRIER
CARLINI
DELISLE
LA HIRE
LAMBERT
EULER
BRAYLEY
PYTHEAS
MARE IMBRIUM
0
200
KILOMETERS
48° N
44°
40°
36°
32°
28°
24°
20°
16° N
38° W
34°
30°
26°
22°
18°
14° W

Figure 1b.

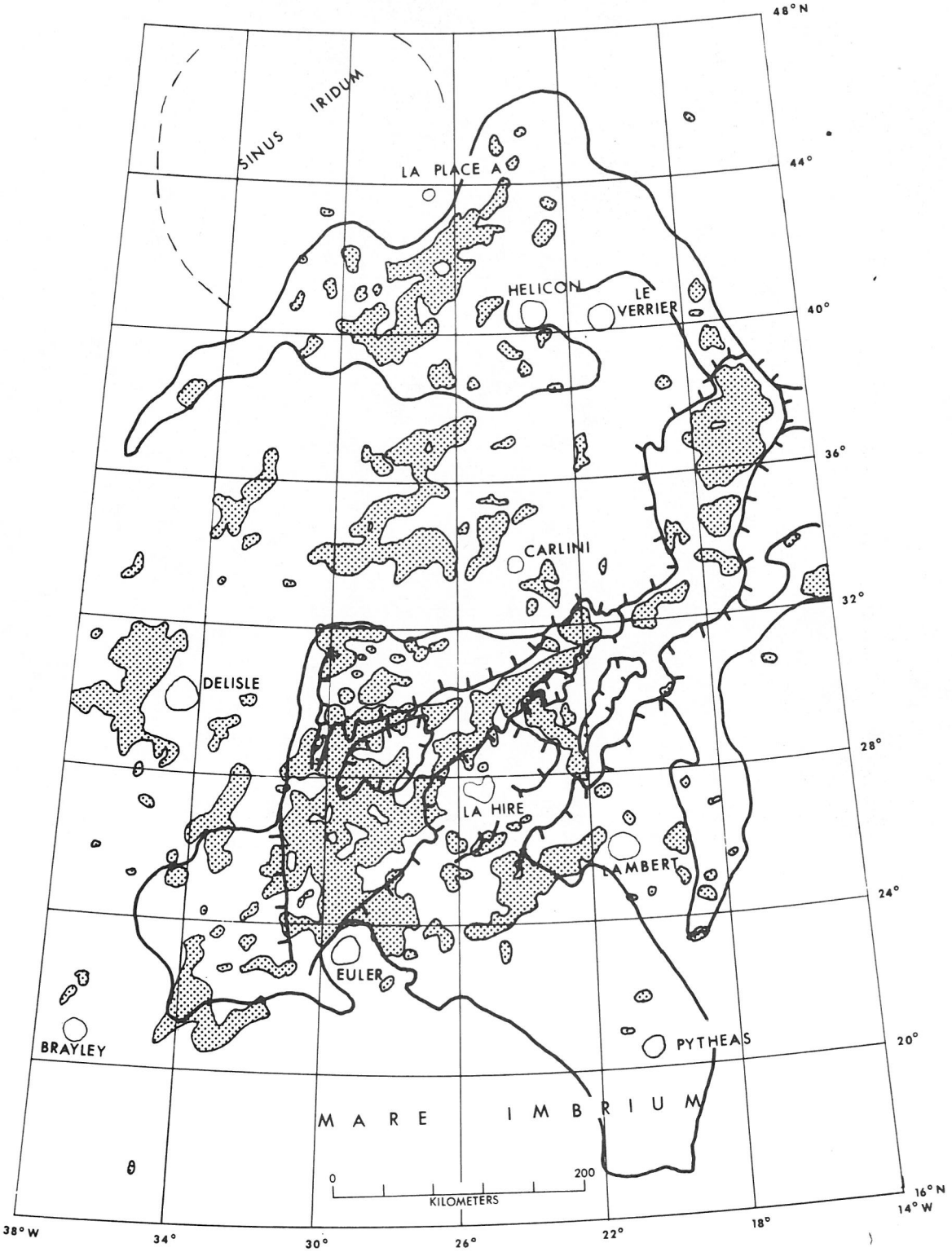
48° N
44°
40°
36°
32°
28°
24°
20°
16° N
14° W
18°
22°
26°
30°
34°
38° W
SINUS IRIDUM
LA PLACE A
HELICON
LE VERRIER
CARLINI
DELISLE
LA HIRE
LAMBERT
EULER
BRAYLEY
PYTHEAS
MARE IMBRIUM
0
200
KILOMETERS

Figure 1c.

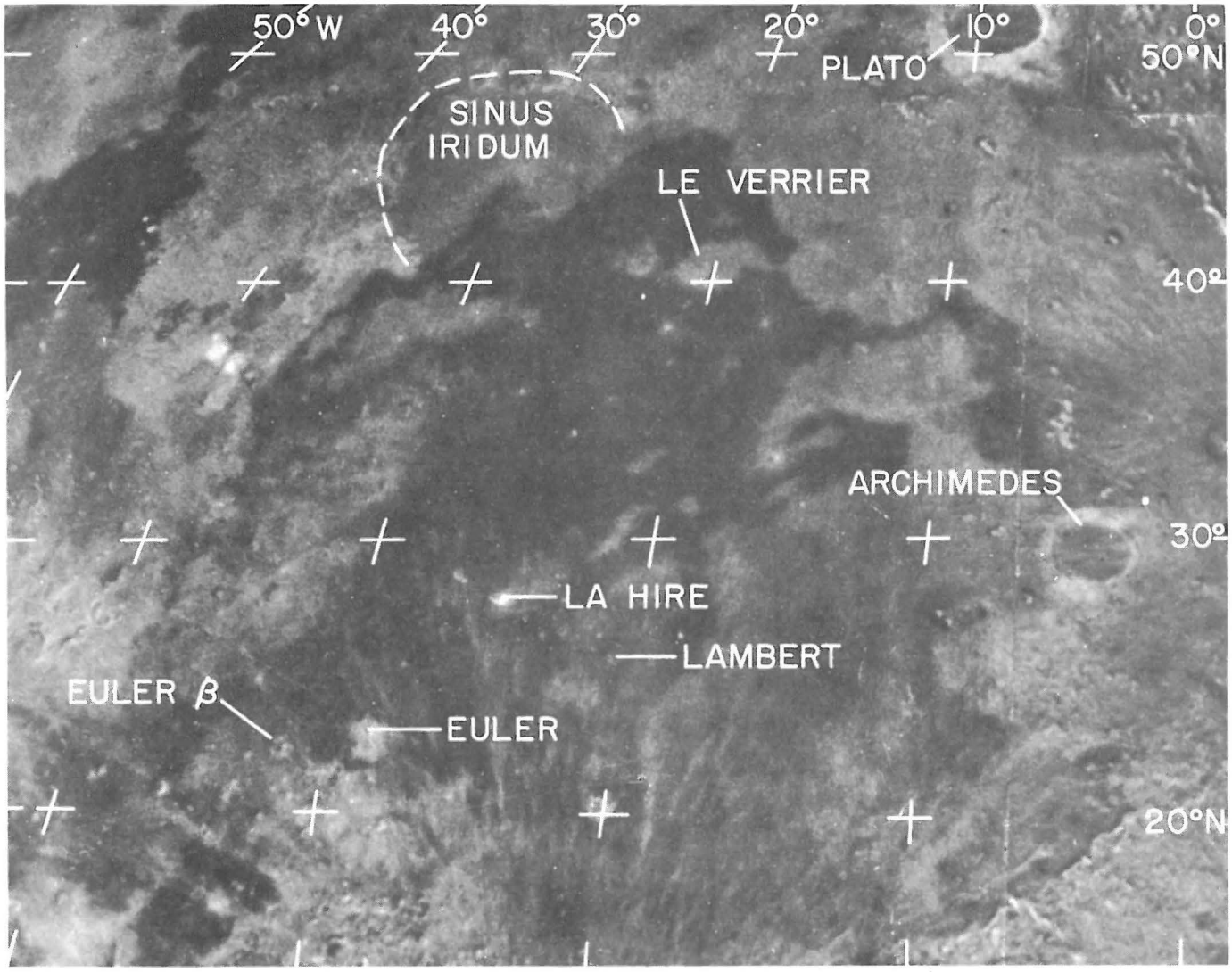
50° W
40°
30°
20°
10°
0°
50°N
PLATO
SINUS
IRIDUM
LE VERRIER
40°
ARCHIMEDES
30°
LA HIRE
LAMBERT
EULER β
EULER
20°N

Figure 2.

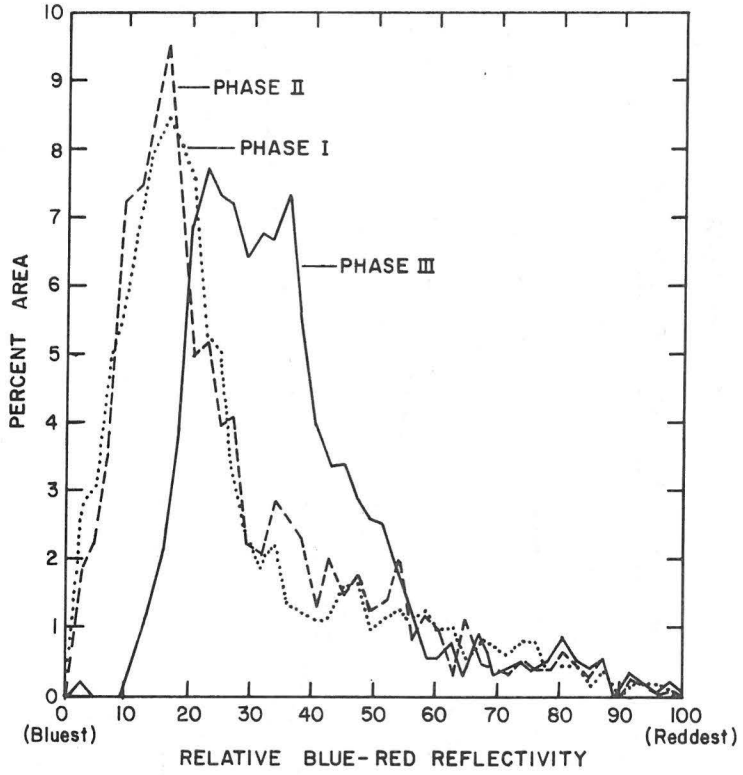
PHASE II
PHASE I
PHASE III
PERCENT AREA
0
1
2
3
4
5
6
7
8
9
10
0
(Bluest)
10
20
30
40
50
60
70
80
90
100
(Reddest)
RELATIVE BLUE-RED REFLECTIVITY

Figure 3a.

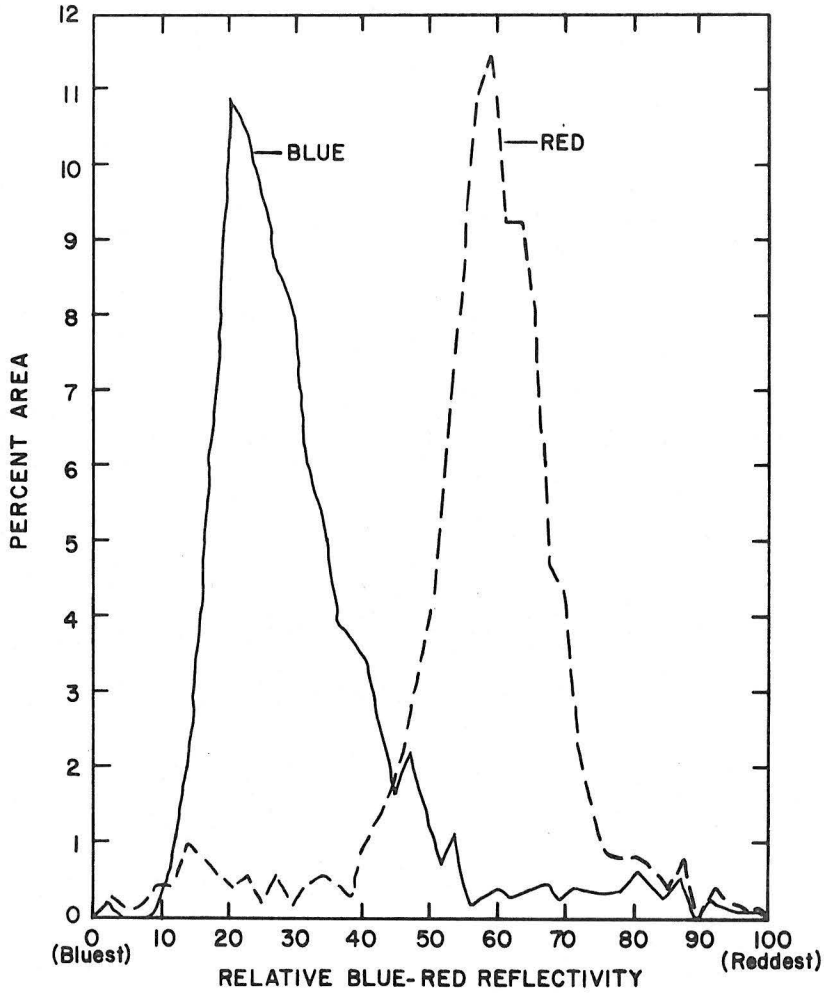
12
11
10
9
8
7
6
5
4
3
2
1
0
PERCENT AREA
BLUE
RED
0
(Bluest)
10
20
30
40
50
60
70
80
90
100
(Reddest)
RELATIVE BLUE-RED REFLECTIVITY

Figure 3b.

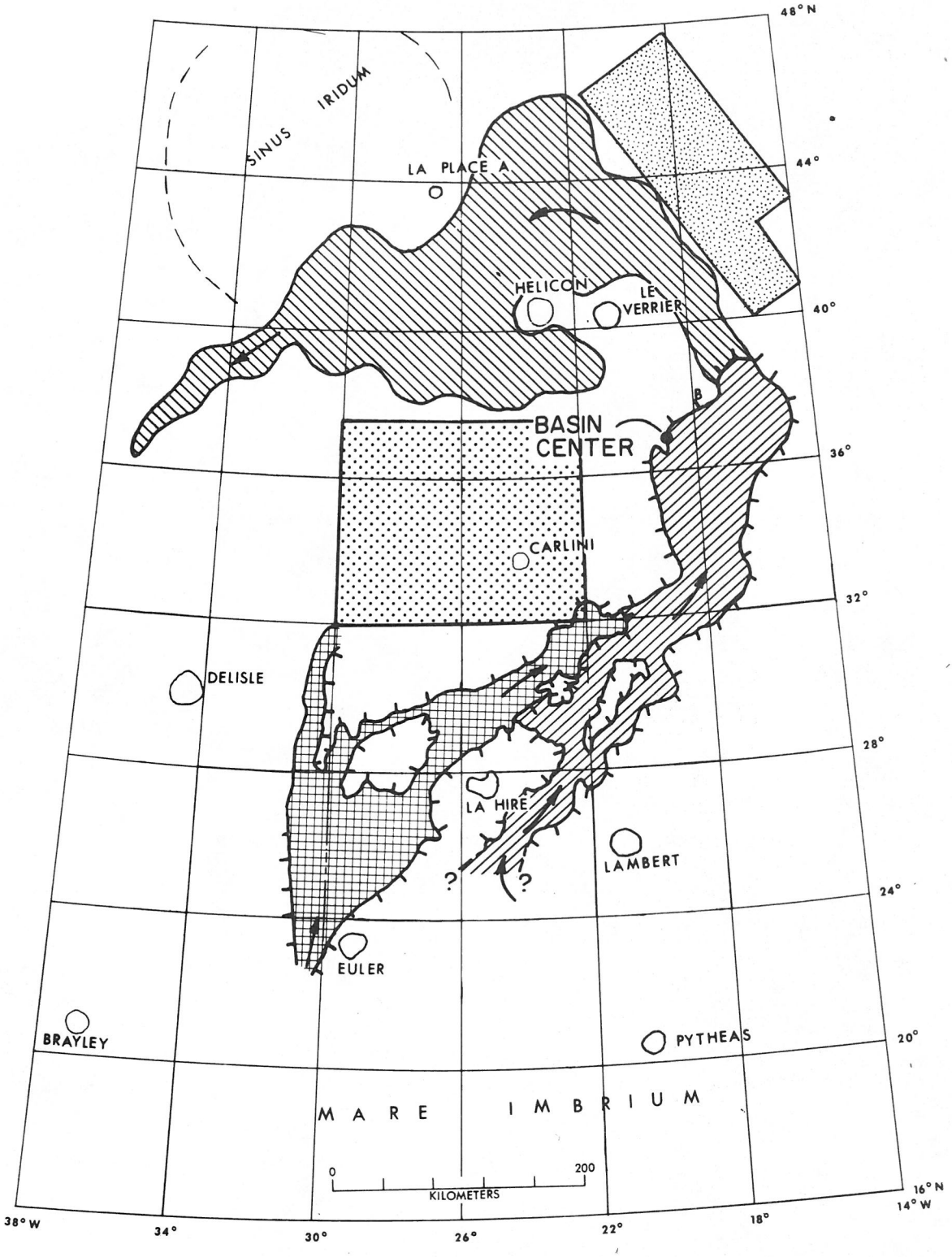
48° N
44°
40°
36°
32°
28°
24°
20°
16° N
14° W
38° W
34°
30°
26°
22°
18°
SINUS IRIDUM
LA PLACE A
HELICON
LE VERRIER
B
BASIN CENTER
CARLINI
DELISLE
LA HIRE
LAMBERT
EULER
BRAYLEY
PYTHEAS
MARE IMBRIUM
0
200
KILOMETERS

Figure 4.

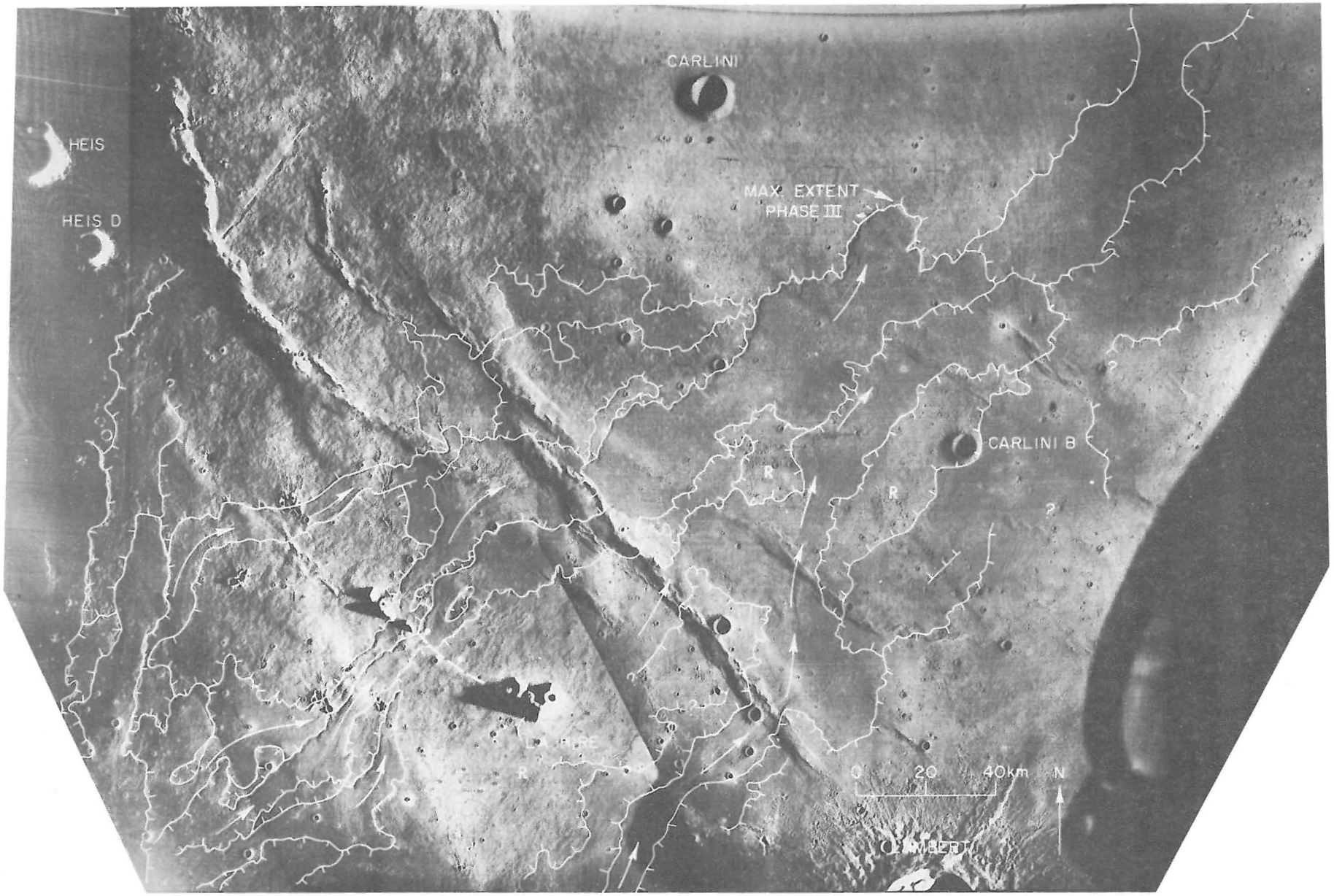
CARLINI
HEIS
HEIS D
MAX. EXTENT
PHASE III
CARLINI B
R
R
R
0 20 40km
N

Figure 5a.

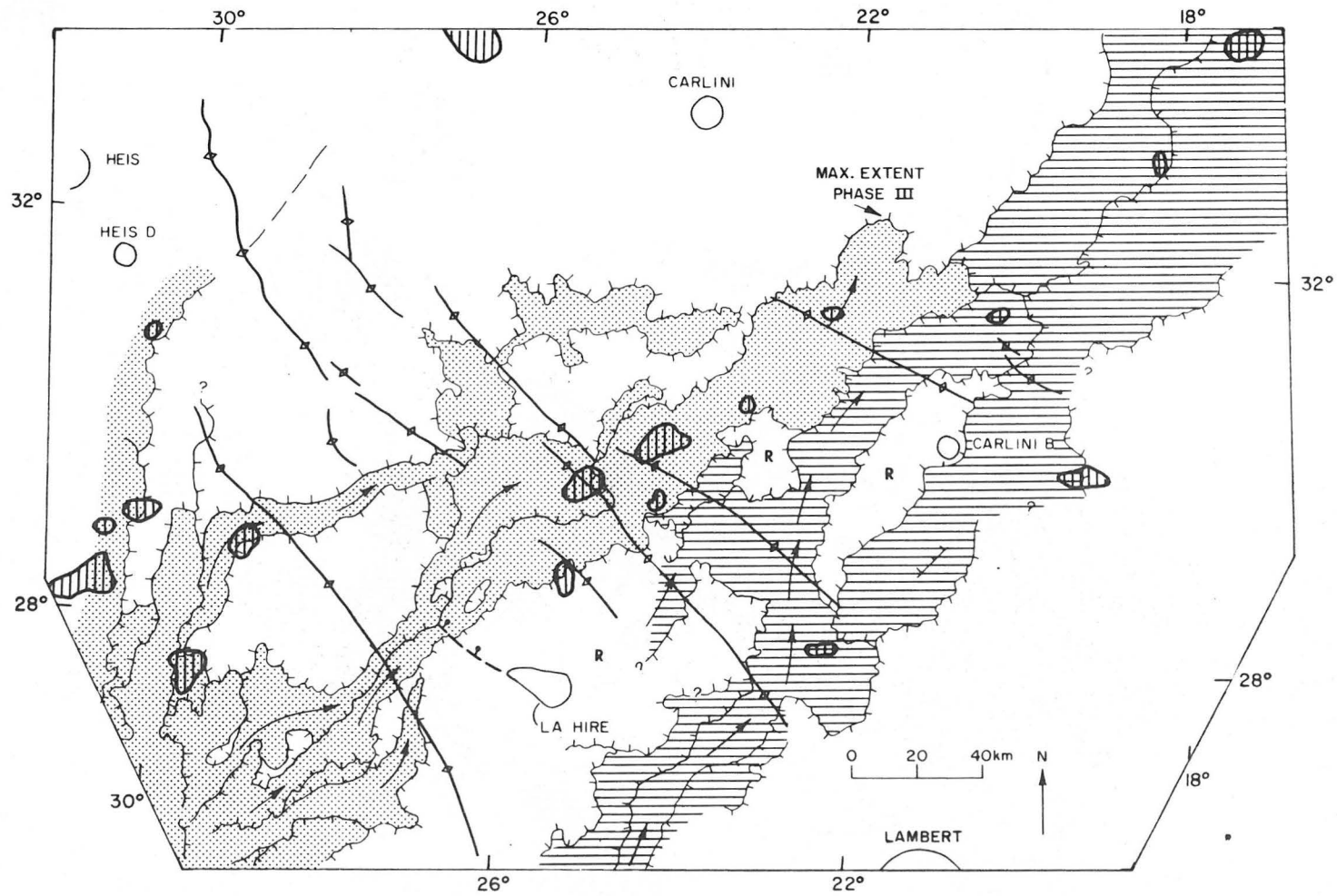
30°
26°
22°
18°
32°
28°
CARLINI
HEIS
HEIS D
MAX. EXTENT
PHASE III
CARLINI B
R
R
R
LA HIRE
0 20 40km
N
LAMBERT

Figure 5b.

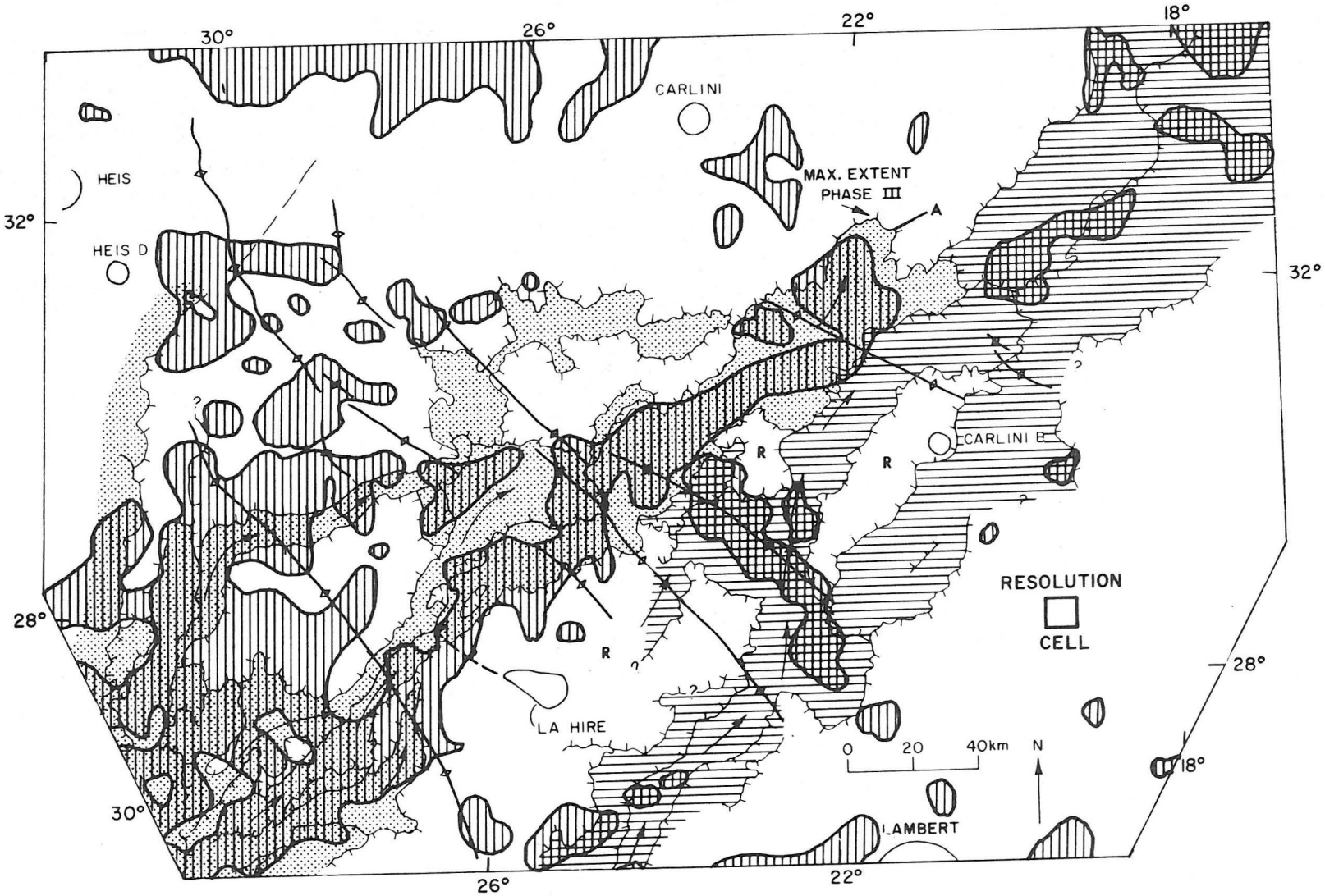
30°
26°
22°
18°
32°
28°
CARLINI
HEIS
HEIS D
MAX. EXTENT
PHASE III
A
CARLINI B
R
R
R
RESOLUTION
CELL
LA HIRE
0 20 40km
N
LAMBERT

Figure 5c.

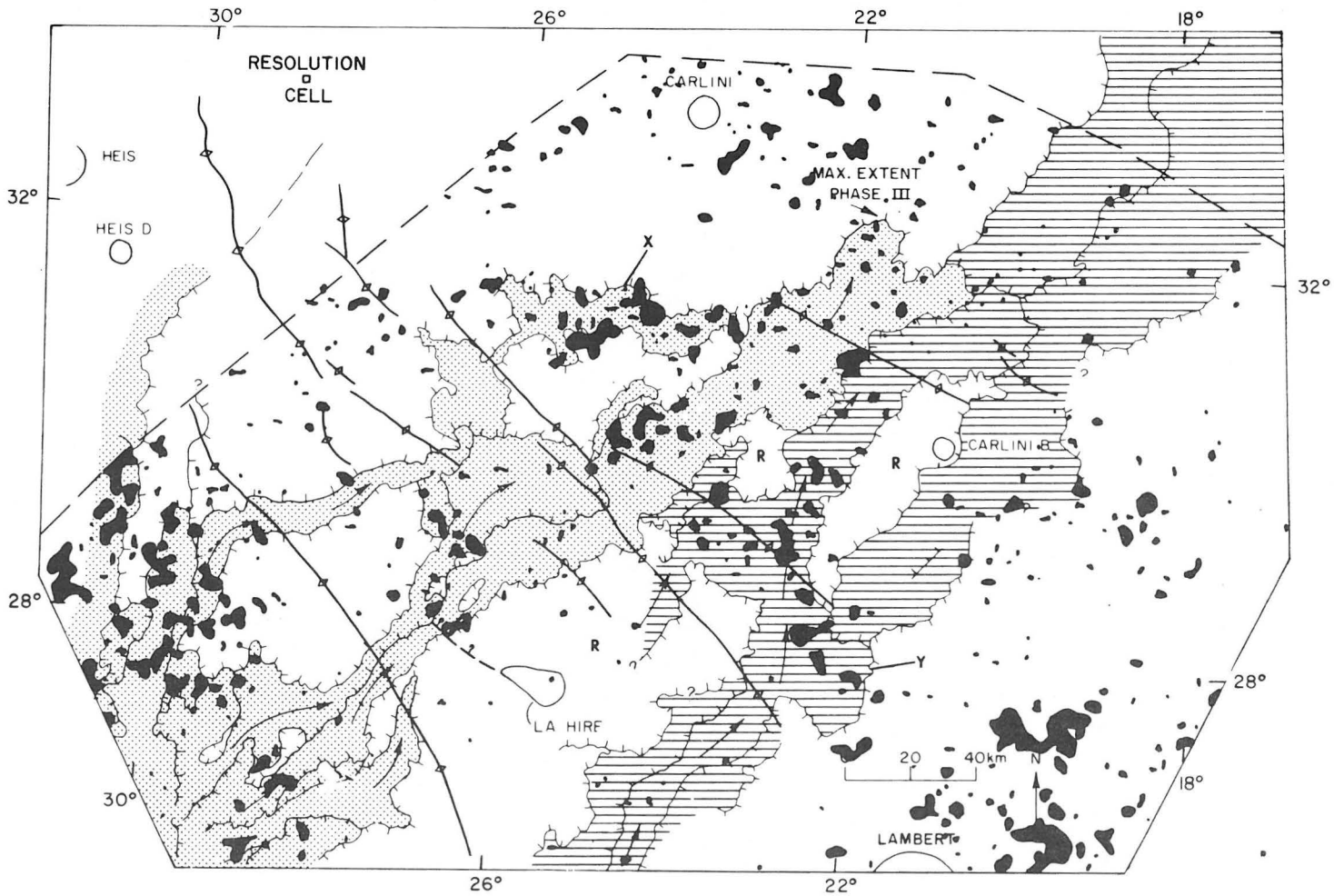
30°
26°
22°
18°
32°
28°
RESOLUTION
CELL
HEIS
HEIS D
CARLINI
MAX. EXTENT
PHASE III
X
Y
R
R
R
CARLINI B
LA HIRE
20
40km
N
LAMBERT

Figure 6.

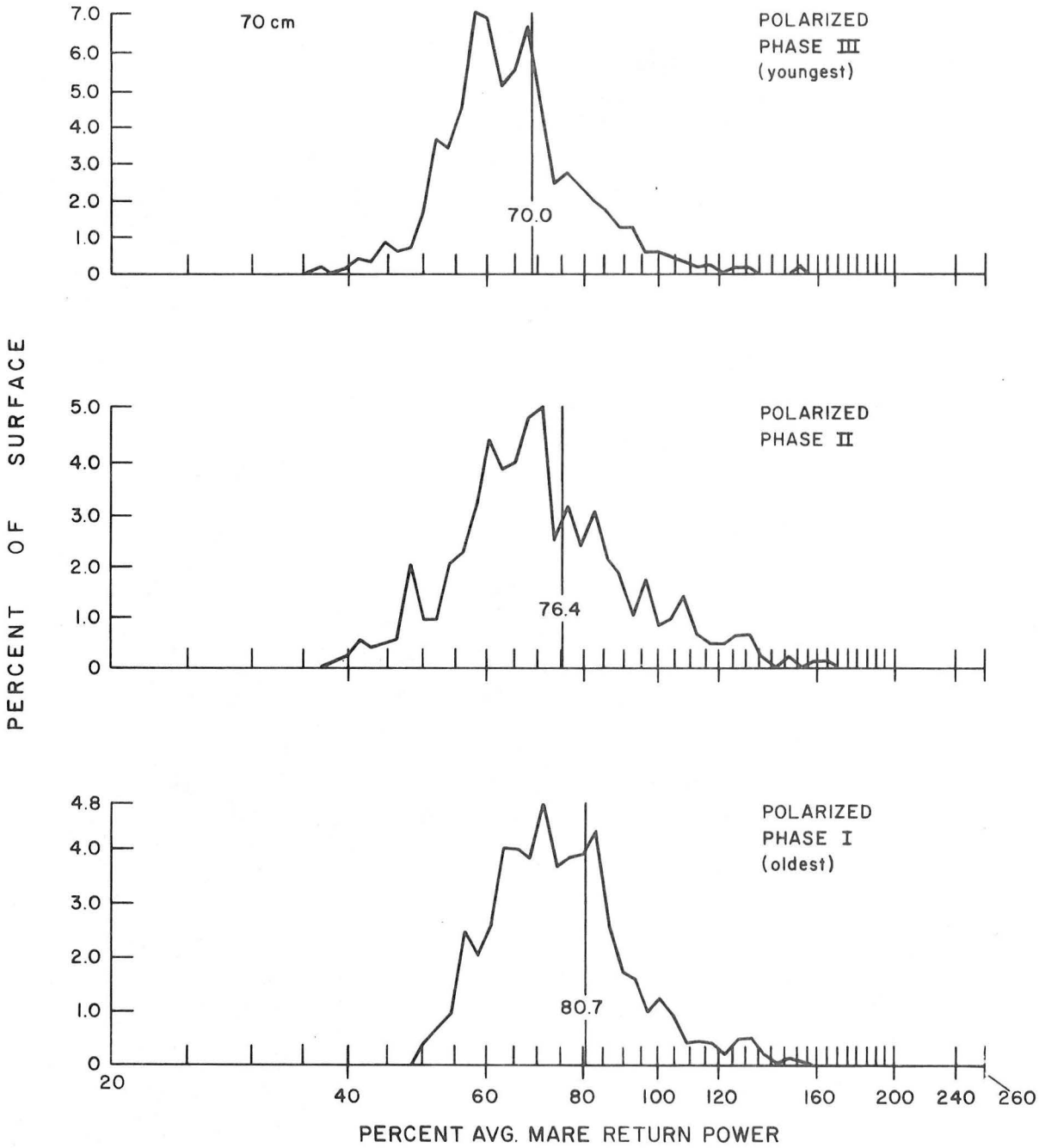
70 cm
POLARIZED
PHASE III
(youngest)
70.0
POLARIZED
PHASE II
76.4
POLARIZED
PHASE I
(oldest)
80.7
PERCENT OF SURFACE
PERCENT AVG. MARE RETURN POWER
7.0
6.0
5.0
4.0
3.0
2.0
1.0
0
4.8
20
40
60
80
100
120
160
200
240
260

Figure 7a.

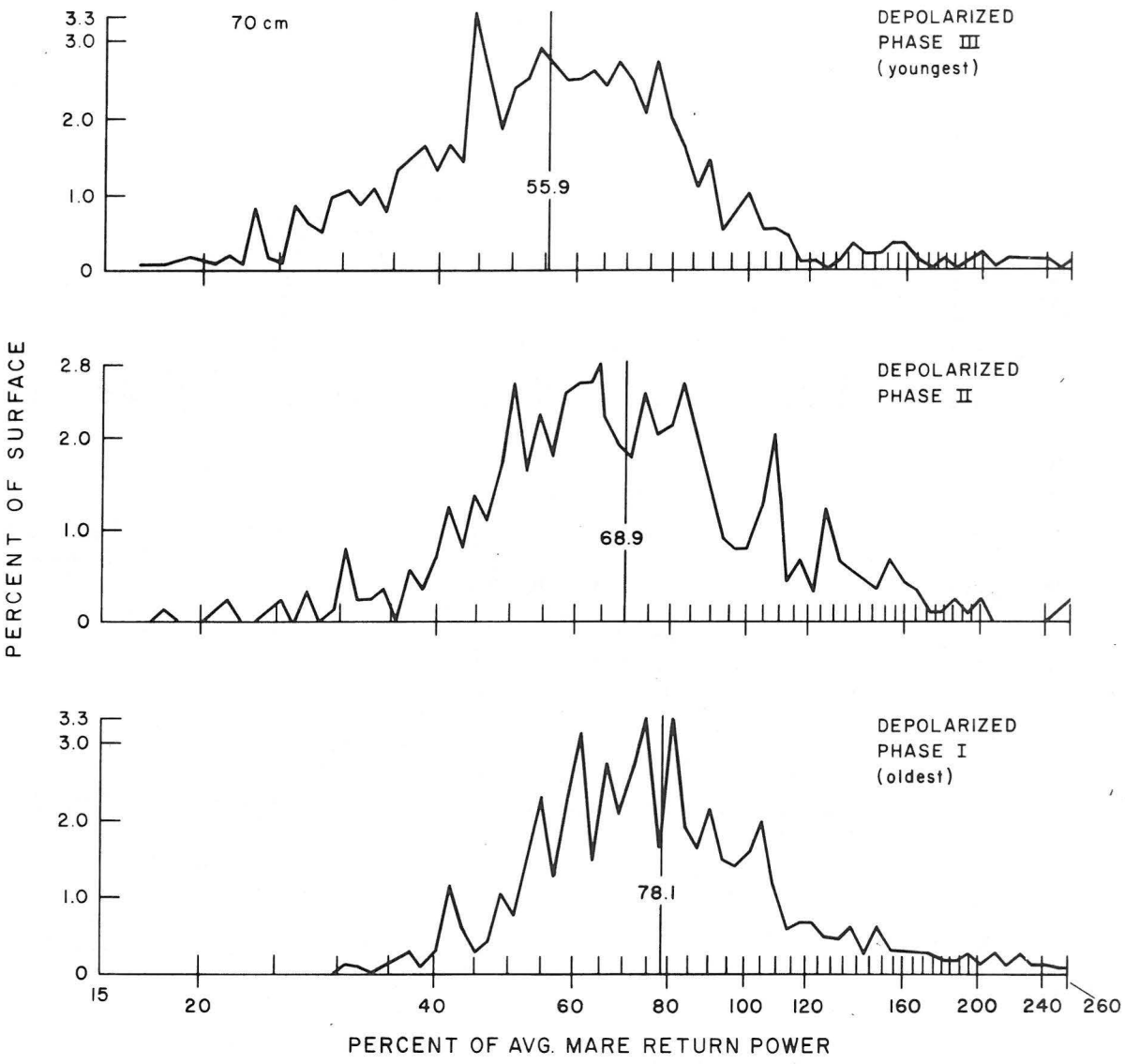
70 cm
DEPOLARIZED
PHASE III
(youngest)
55.9
DEPOLARIZED
PHASE II
68.9
DEPOLARIZED
PHASE I
(oldest)
78.1
PERCENT OF SURFACE
PERCENT OF AVG. MARE RETURN POWER
3.3
3.0
2.8
2.0
1.0
0
15
20
40
60
80
100
120
160
200
240
260

Figure 7b.

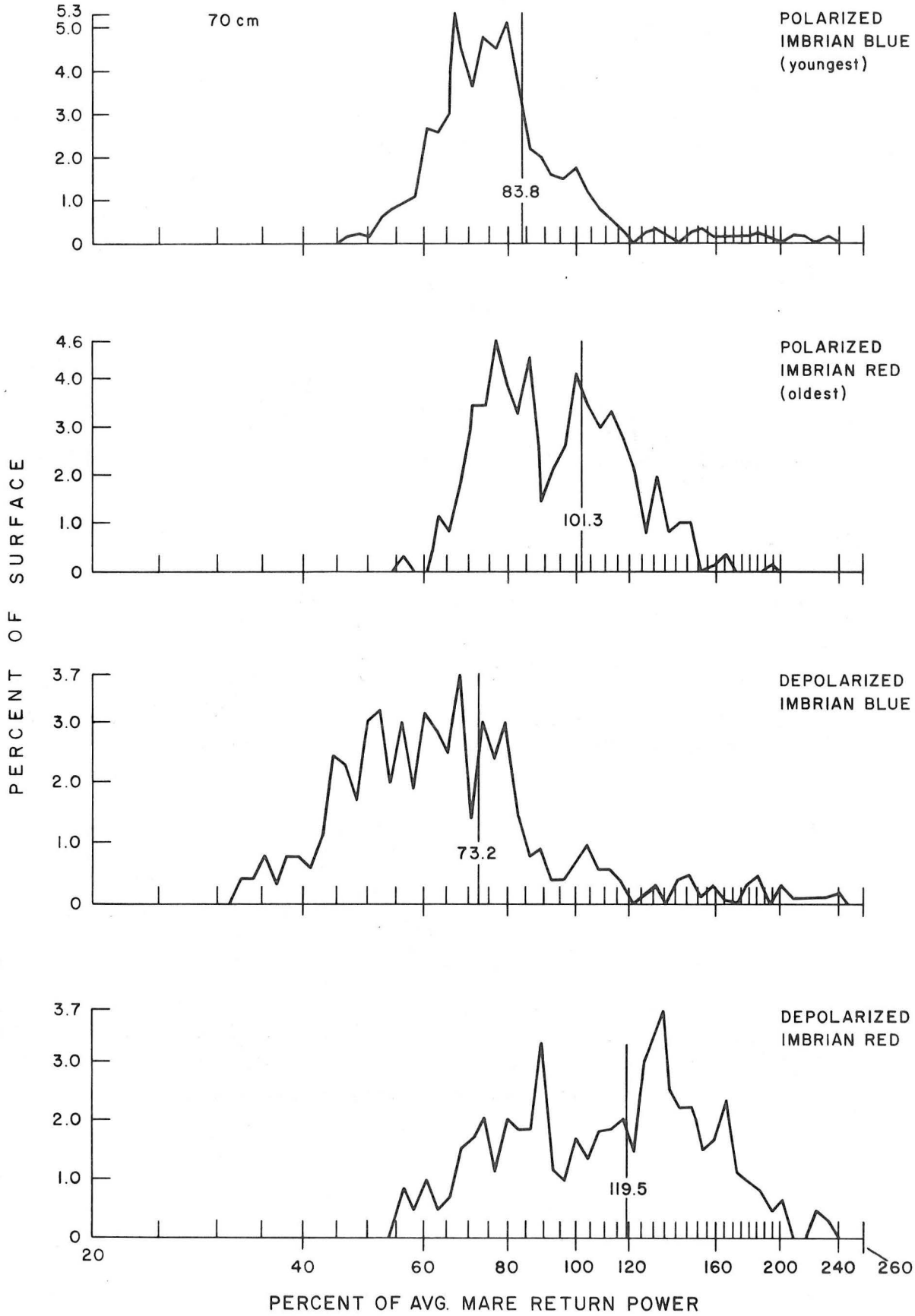
70 cm
POLARIZED
IMBRIAN BLUE
(youngest)
83.8
POLARIZED
IMBRIAN RED
(oldest)
101.3
DEPOLARIZED
IMBRIAN BLUE
73.2
DEPOLARIZED
IMBRIAN RED
119.5
PERCENT OF SURFACE
PERCENT OF AVG. MARE RETURN POWER
5.3
5.0
4.0
3.0
2.0
1.0
0
4.6
3.7
20
40
60
80
100
120
160
200
240
260

Figure 7c.

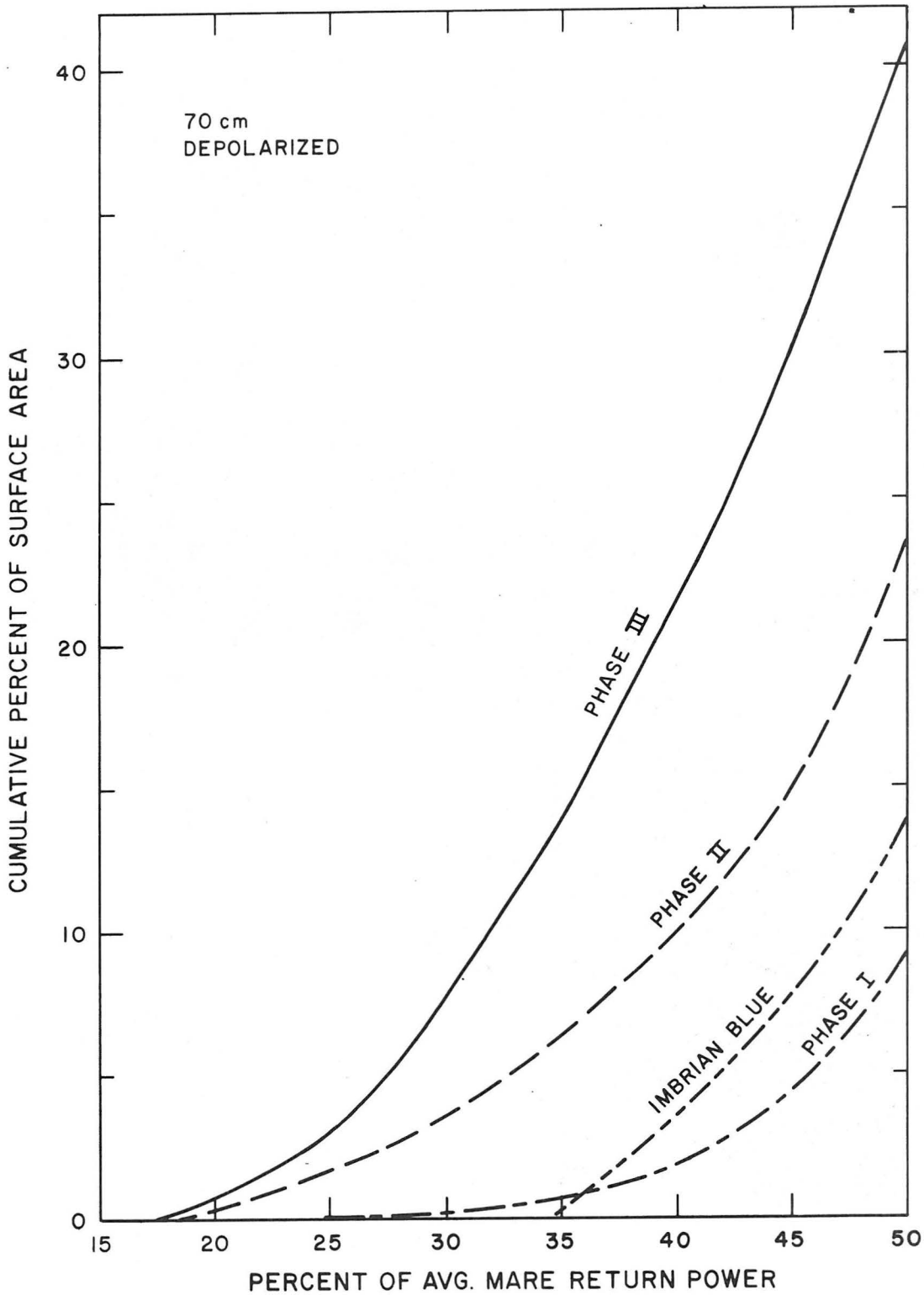
70 cm
DEPOLARIZED
PHASE III
PHASE II
IMBRIAN BLUE
PHASE I
CUMULATIVE PERCENT OF SURFACE AREA
0
10
20
30
40
15
20
25
30
35
40
45
50
PERCENT OF AVG. MARE RETURN POWER

Figure 8.

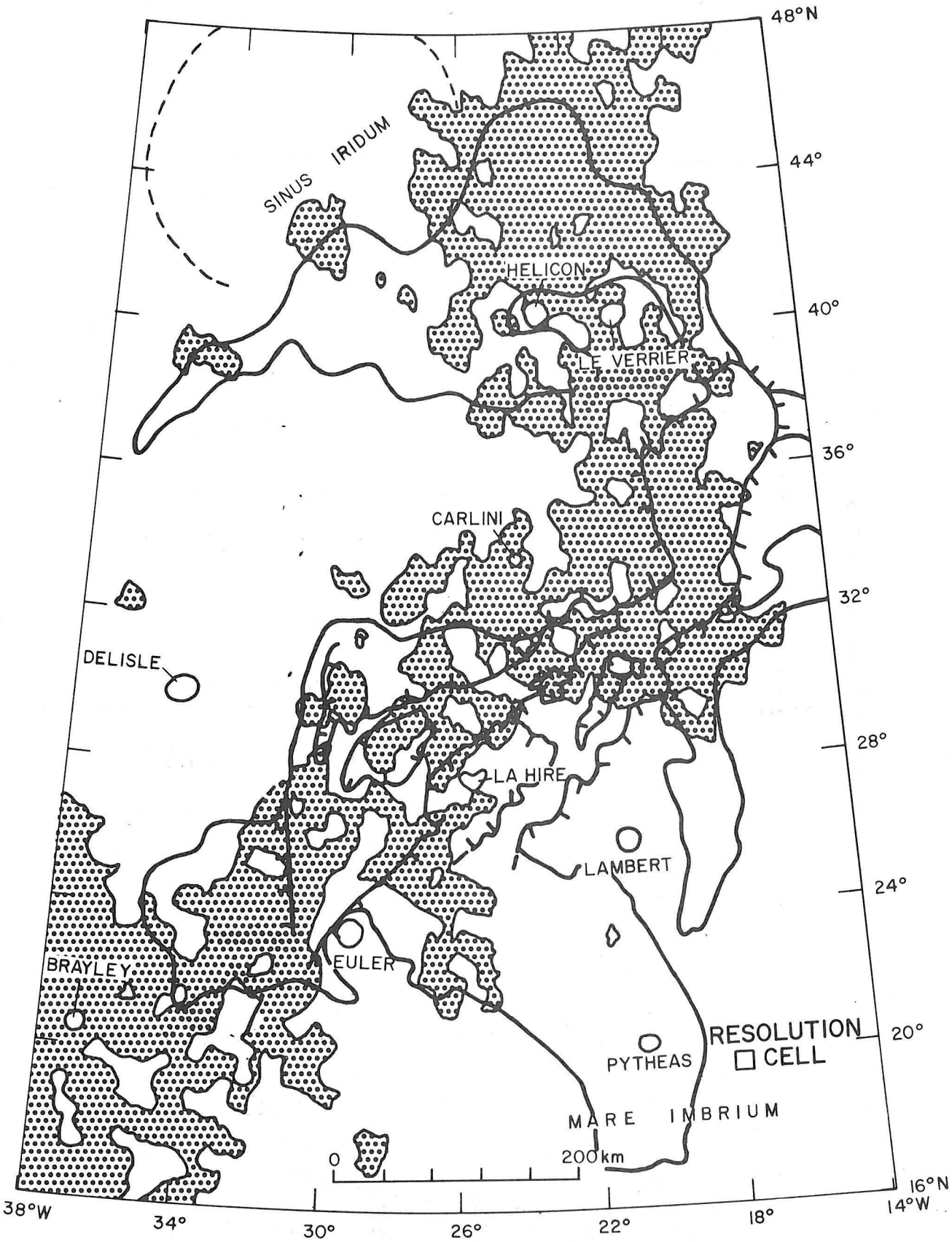
48°N
44°
40°
36°
32°
28°
24°
20°
16°N
38°W
34°
30°
26°
22°
18°
14°W
SINUS IRIDUM
HELICON
LE VERRIER
CARLINI
DELISLE
LA HIRE
LAMBERT
EULER
BRAYLEY
PYTHEAS
RESOLUTION CELL
MARE IMBRIUM
0
200 km

Figure 9.

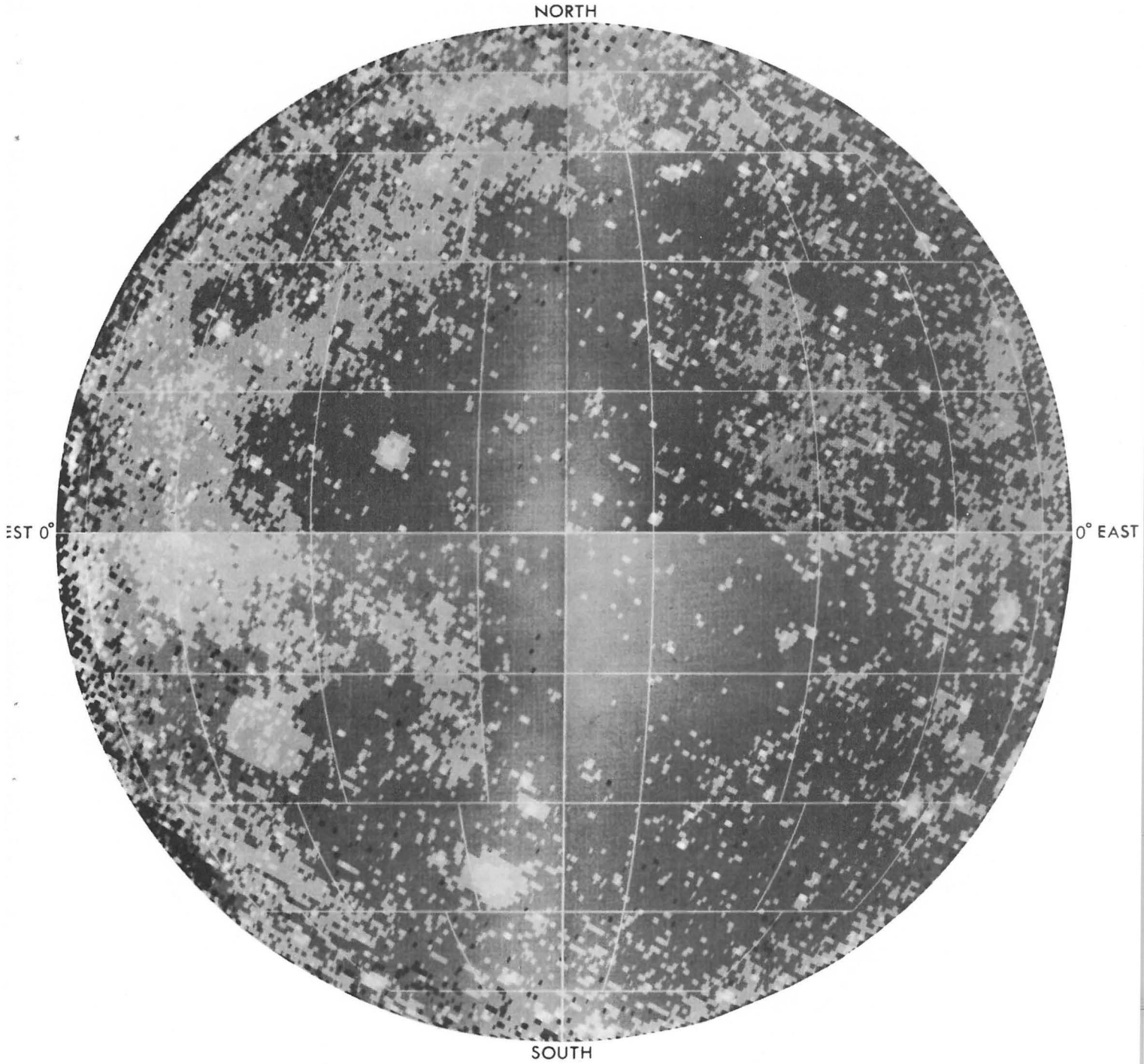

Figure 10a.

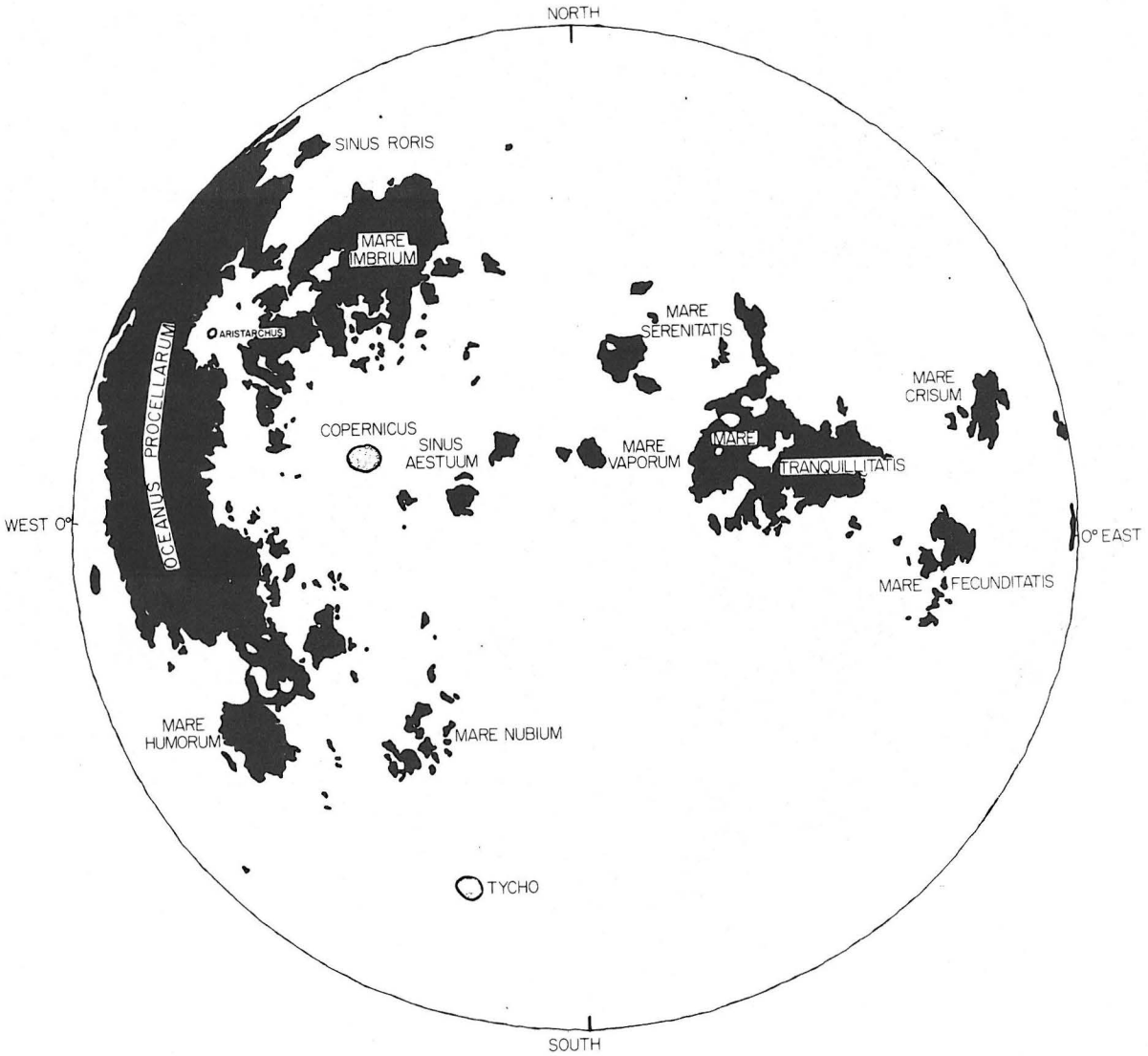
NORTH
SINUS RORIS
MARE IMBRIUM
ARISTARCHUS
OCEANUS PROCELLARUM
MARE SERENITATIS
MARE CRISUM
COPERNICUS
SINUS AESTUUM
MARE VAPORUM
MARE TRANQUILLITATIS
WEST 0°
0° EAST
MARE FECUNDITATIS
MARE HUMORUM
MARE NUBIUM
TYCHO
SOUTH

Figure 10b.

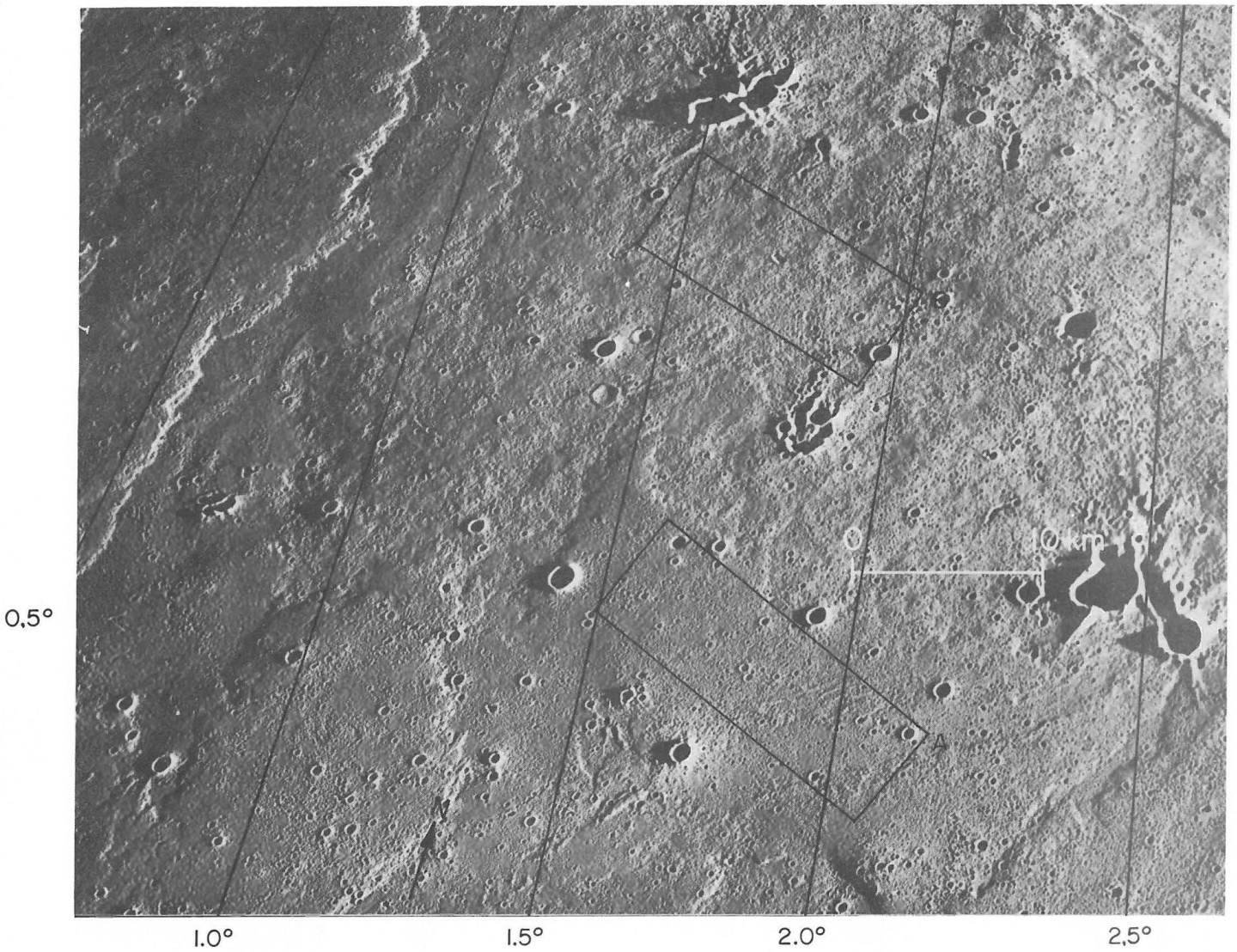

Figure 11.

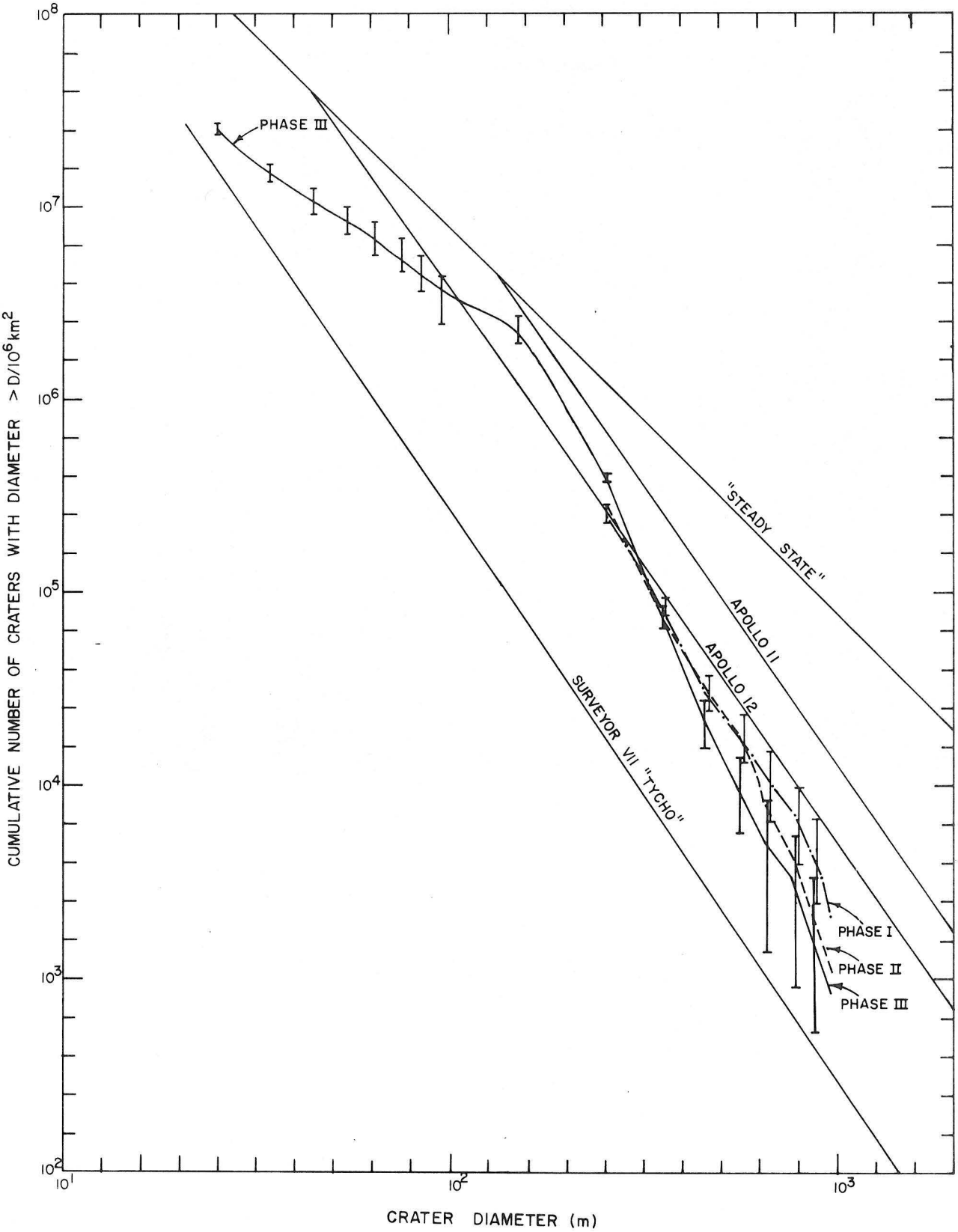
CUMULATIVE NUMBER OF CRATERS WITH DIAMETER > D/10^6 km^2
CRATER DIAMETER (m)
PHASE III
"STEADY STATE"
APOLLO 11
APOLLO 12
SURVEYOR VII "TYCHO"
PHASE I
PHASE II
PHASE III

Figure 12a.

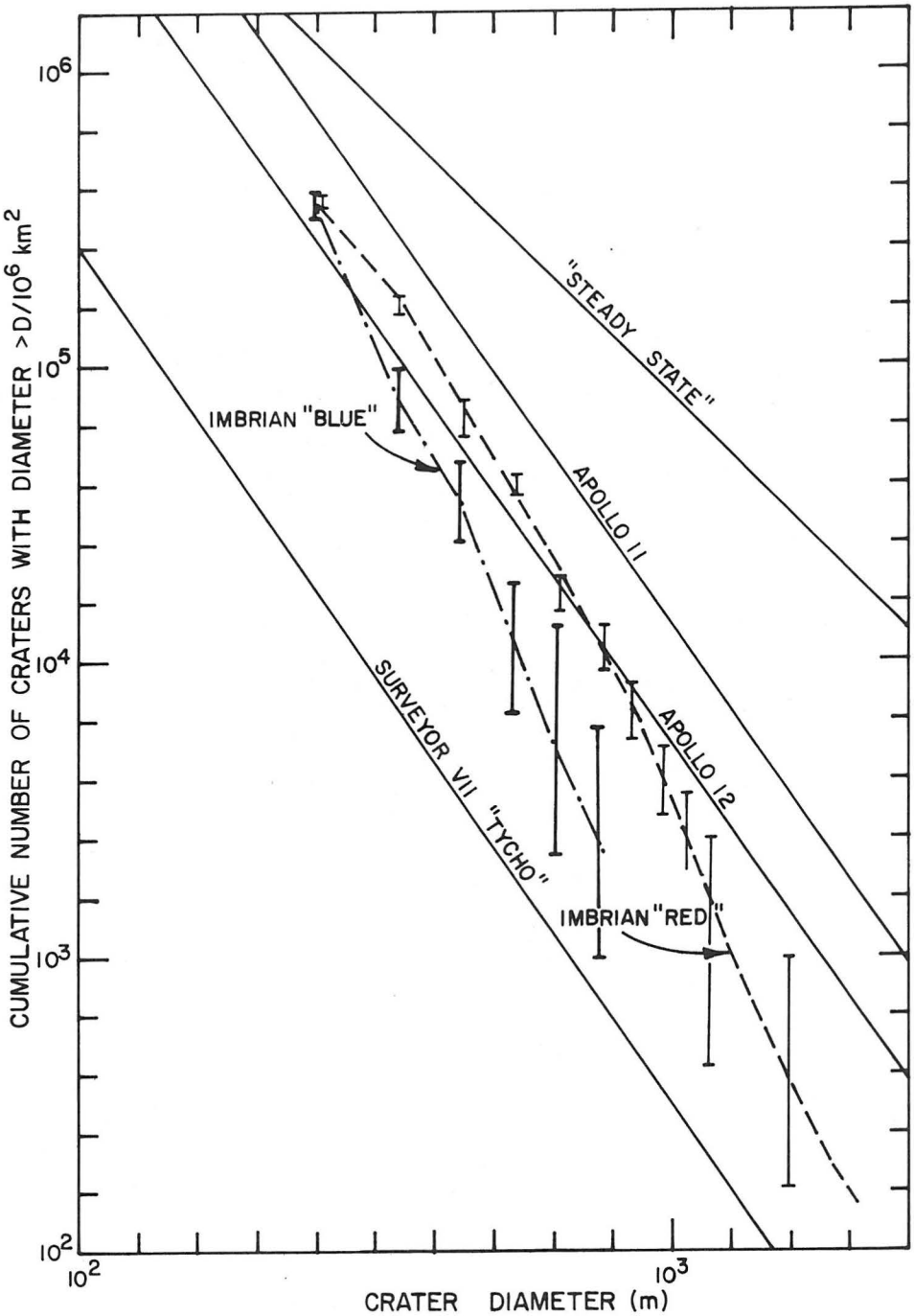
CUMULATIVE NUMBER OF CRATERS WITH DIAMETER >D/10^6 km^2
10^6
10^5
10^4
10^3
10^2
10^2
10^3
CRATER DIAMETER (m)
"STEADY STATE"
APOLLO 11
APOLLO 12
SURVEYOR VII "TYCHO"
IMBRIAN "BLUE"
IMBRIAN "RED"

Figure 12b.

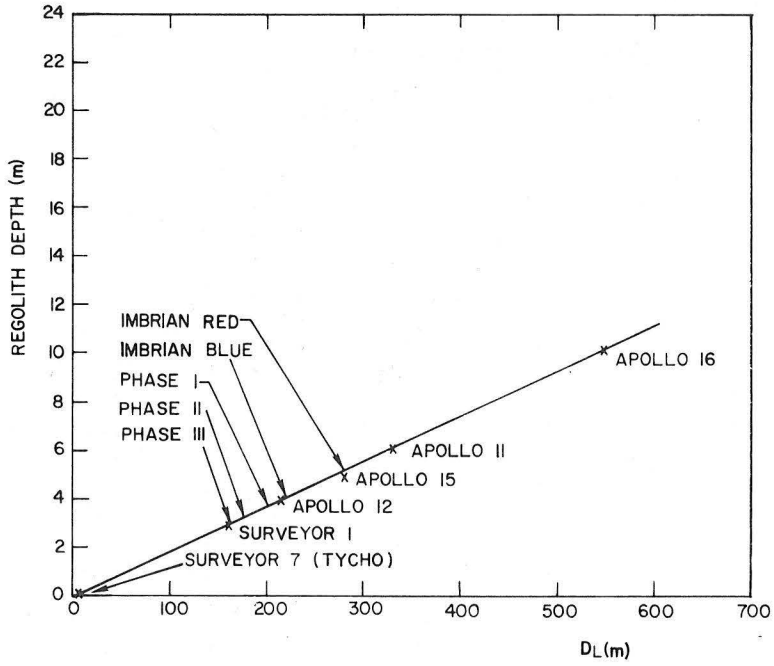
REGOLITH DEPTH (m)
24
22
20
18
16
14
12
10
8
6
4
2
0
0
100
200
300
400
500
600
700
DL(m)
IMBRIAN RED
IMBRIAN BLUE
PHASE I
PHASE II
PHASE III
APOLLO 16
APOLLO 11
APOLLO 15
APOLLO 12
SURVEYOR I
SURVEYOR 7 (TYCHO)

Figure 13.

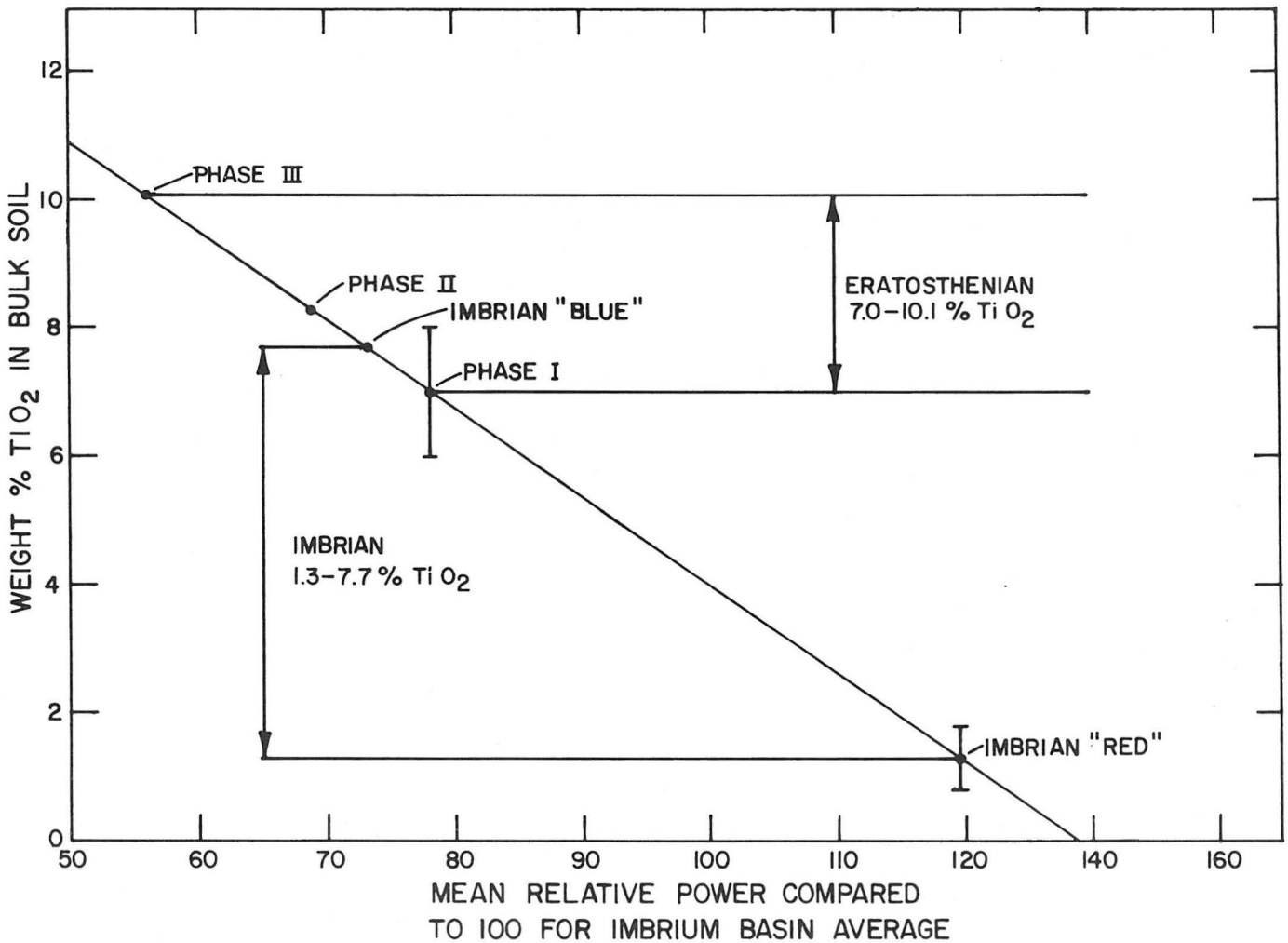
WEIGHT % TiO_2 IN BULK SOIL
0
2
4
6
8
10
12
50
60
70
80
90
100
110
120
140
160
MEAN RELATIVE POWER COMPARED
TO 100 FOR IMBRIUM BASIN AVERAGE
PHASE III
PHASE II
IMBRIAN "BLUE"
PHASE I
ERATOSTHENIAN
7.0–10.1 % TiO_2
IMBRIAN
1.3–7.7 % TiO_2
IMBRIAN "RED"

Figure 14.

TABLE 1

70 cm polarized and depolarized radar statistics for Imbrian and Eratosthenian mare surfaces within Mare Imbrium

Mare unit	Percent of avg. polarized power for basin(avg.=100)	Standard deviation	Percent of avg. depolarized power for basin(avg.=100)	Standard deviation	Percent of mare unit area with < 50 percent of avg. depolarized power for basin
ERATOSTHENIAN					
phase III (youngest)	70.0	10.7	55.9	23.6	40.7
phase II	76.4	14.1	68.9	25.0	23.3
phase I	80.7	11.5	78.1	20.1	9.3
IMBRIAN					
Imbrian blue	83.8	13.3	73.2	22.1	13.9
Imbrian red (oldest)	101.3	13.0	119.5	18.4	0.0